Siglec-H is a microglia-specific marker that discriminates microglia from CNS-associated macrophages and CNS-infiltrating monocytes

Running title: Siglec-H is a specific marker for microglia

Hiroyuki Konishi[1], Masaaki Kobayashi[1], Taikan Kunisawa[1], Kenta Imai[1], Akira Sayo[1,2], Bernard Malissen[3], Paul R. Crocker[4], Katsuaki Sato[5], Hiroshi Kiyama[1]

[1]Department of Functional Anatomy and Neuroscience, Nagoya University Graduate School of Medicine, Nagoya 466-8550, Japan
[2]Department of Oral and Maxillofacial Surgery, Nagoya University Graduate School of Medicine, Nagoya 466-8550, Japan
[3]Centre d'Immunologie de Marseille-Luminy, Aix Marseille Université, INSERM, CNRS UMR, Marseille 13288, France
[4]Division of Cell Signalling and Immunology, School of Life Sciences, University of Dundee, Dundee DD1 5EH, United Kingdom
[5]Division of Immunology, Department of Infectious Diseases, Faculty of Medicine, University of Miyazaki, 5200 Kihara, Kiyotake 889-1692, Japan

E-mail addresses:
Hiroyuki Konishi: konishi@med.nagoya-u.ac.jp
Masaaki Kobayashi: 4444.forum@gmail.com
Taikan Kunisawa: t.k.227.ytn@gmail.com
Kenta Imai: imaken0311@yahoo.co.jp
Akira Sayo: akira.sayo@med.nagoya-u.ac.jp
Bernard Malissen: bernardm@ciml.univ-mrs.fr
Paul R. Crocker: p.r.crocker@dundee.ac.uk
Katsuaki Sato: katsuaki_sato@med.miyazaki-u.ac.jp
Hiroshi Kiyama: kiyama@med.nagoya-u.ac.jp

Corresponding authors:
Hiroyuki Konishi and Hiroshi Kiyama, Department of Functional Anatomy and Neuroscience, 65, Tsurumai-cho, Showa-ku, Nagoya 466-8550, Japan, Tel.: +81-52-744-2015, Fax: +81-52-744-2027, E-mail: konishi@med.nagoya-u.ac.jp, kiyama@med.nagoya-u.ac.jp

Number of words: 247 (Abstract), 676 (Introduction), 1779 (Materials and Methids), 2393 (Results), 1511 (Discussion), 117 (Acknowledgments), 2463 (References), 1695 (Figure legends) and 10881 (Total)

Number of figures: 7 (+ 1 supplemental figure)

Number of tables: 0

Main points:

1. Siglec-H is expressed by microglia including during developmental stages in mice.
2. Siglec-H expression is largely absent from other types of myeloid cells in the CNS, such as CNS-associated macrophages and CNS-infiltrating monocytes.

Key words:
allodynia, choroid plexus, inflammation, meninges, myeloid cells, pain, perivascular spaces

Abstract

Several types of myeloid cell are resident in the CNS. In the steady state, microglia are present in the CNS parenchyma, whereas macrophages reside in boundary regions of the CNS, such as perivascular spaces, the meninges and choroid plexus. In addition, monocytes infiltrate into the CNS parenchyma from circulation upon blood–brain barrier breakdown after CNS injury and inflammation. Although several markers, such as CD11b and ionized calcium-binding adapter molecule 1 (Iba1), are frequently used as microglial markers, they are also expressed by other types of myeloid cell and microglia-specific markers were not defined until recently. Previous transcriptome analyses of isolated microglia identified a transmembrane lectin, sialic acid-binding immunoglobulin-like lectin H (Siglec-H), as a molecular signature for microglia; however, this was not confirmed by histological studies in the nervous system and the reliability of Siglec-H as a microglial marker remained unclear. Here, we demonstrate that Siglec-H is an authentic marker for microglia in mice by immunohistochemistry using a Siglec-H-specific antibody. Siglec-H was expressed by parenchymal microglia from developmental stages to adulthood, and the expression was maintained in activated microglia under injury or inflammatory condition. However, Siglec-H expression was absent from CNS-associated macrophages and CNS-infiltrating monocytes, except for a minor subset of cells. We also show that the *Siglech* gene locus is a feasible site for specific targeting of microglia in the nervous system. In conclusion, Siglec-H is a reliable marker for microglia that will allow histological identification of microglia and microglia-specific gene manipulation in the nervous system.

Introduction

Microglia are mononuclear phagocytes in the CNS parenchyma. They originate from erythromyeloid precursors in the yolk sac and then migrate to the CNS during the embryonic stage to reside in the parenchyma (Ginhoux et al., 2010; Gomez Perdiguero et al., 2015; Hoeffel et al., 2015; Kierdorf et al., 2013; Schulz et al., 2012). Microglia play roles in various events, such as formation of neuronal circuits (Paolicelli et al., 2011; Schafer et al., 2012) and neuronal degeneration/regeneration after neuronal injury (Gamo et al., 2008; Kobayashi, Konishi, Takai, & Kiyama, 2015; Konishi, Namikawa, & Kiyama, 2006; Kroner et al., 2014). Although microglia are a well-known type of CNS myeloid cell, other types of myeloid cell also reside at the boundaries of the CNS (Galea et al., 2005; Goldmann et al., 2016; Prinz, Erny, & Hagemeyer, 2017; Prinz & Priller, 2014), including perivascular macrophages (MΦ, pvMΦ) in the perivascular space around medium- or large-sized vessels, meningeal MΦ (mMΦ) in the meninges, and choroid plexus MΦ (cpMΦ) in the choroid plexus. In addition to these "CNS-associated MΦ", monocytes infiltrate into the CNS parenchyma from the blood circulation upon blood–brain barrier breakdown under injury or inflammatory conditions (King, Dickendesher, & Segal, 2009; Mildner et al., 2009; Saederup et al., 2010; Varvel et al., 2016).

Several molecules including CD11b and ionized calcium-binding adapter molecule 1 (Iba1) were established as microglial markers, and antibodies against CD11b and Iba1 were frequently used for immunohistochemical identification of microglia (Ito et al., 1998; Robinson, White, & Mason, 1986). However, CD11b and Iba1 are widely expressed by myeloid cell types (Ajami et al., 2011; Greter, Lelios, & Croxford, 2015; Prinz & Priller, 2014; Prinz, Priller, Sisodia, & Ransohoff, 2011), meaning that the antibodies cannot discriminate microglia from CNS-associated MΦ and CNS-infiltrating monocytes by immunohistochemistry. For gene targeting of microglia, gene loci or promoter/enhancer regions of *integrin subunit alpha M* (*Itgam*) (encoding CD11b), *colony-stimulating factor 1 receptor* (*Csf1r*) and *C-X3-C motif chemokine receptor 1* (*Cx3cr1*) were utilized (Boillee et al., 2006; Jung et al., 2000; Pfrieger & Slezak, 2012; Sasmono et al., 2003). However, microglia-specific targeting was not achieved because these genes are also expressed by other myeloid populations (Goldmann et al., 2016; Wieghofer, Knobeloch, & Prinz, 2015). Therefore identification of microglia-specific molecules, which are not expressed by other myeloid species, has been pursued.

Several studies have used transcriptome analysis to determine the molecular signature of microglia, resulting in the identification of molecules that are highly expressed by microglia but not by other myeloid cells (Bedard, Tremblay, Chernomoretz, & Vallieres, 2007; Butovsky et al., 2014; Chiu et al., 2013; Gautier et al., 2012; Hickman et al., 2013; Wes et al., 2016). Among the molecules identified, the expression of transmembrane protein 119 (TMEM119) (Bennett et al., 2016), Sall1 (Buttgereit et al., 2016) and $P2Y_{12}$ (Mildner et al.,

2017) histologically discriminated microglia from CNS-associated MΦ or CNS-infiltrating monocytes. Although expression of these molecules is restricted to microglia in the CNS, these markers are not fully specific. For example, TMEM119 expression is absent in immature microglia (Bennett et al., 2016), Sall1 is abundantly expressed in neuronal/glial progenitor cells during development (Buttgereit et al., 2016; Harrison, Nishinakamura, Jones, & Monaghan, 2012), and $P2Y_{12}$ shows decreased/diminished expression in activated microglia (Amadio et al., 2014; Haynes et al., 2006; Mildner et al., 2017).

In this study, we focused on a transmembrane lectin, sialic acid-binding immunoglobulin-like lectin H (Siglec-H), which is known as a marker for plasmacytoid dendritic cells (pDCs) in the immune system (Blasius et al., 2006; Zhang et al., 2006). Previous transcriptome and flow cytometric studies on isolated cells suggested Siglec-H as a microglia-specific molecule that was not expressed by peripheral myeloid cells, such as circulating monocytes and peripheral MΦ (Bedard, Tremblay, Chernomoretz, & Vallieres, 2007; Butovsky et al., 2014; Chiu et al., 2013; Gautier et al., 2012; Hickman et al., 2013). However, no immunohistochemical studies of the nervous system were performed, and marker specificity of Siglec-H, for instance, for CNS-associated MΦ and CNS-infiltrating monocytes, remained unexplored. Here we demonstrated microglia-specific expression of Siglec-H, including during developmental stages and under injury conditions.

Materials and Methods

Animals

C57BL/6J wild-type (WT) mice were purchased from Charles River Laboratories Japan. *Siglech*$^{dtr/dtr}$ mice on a C57BL/6J background are described in our previous study (B6.Cg-*Siglech*$^{<tm1.1Ksat>}$ mice; deposited in RIKEN BioResource Center [accession number: RBRC05658]) (Takagi et al., 2011). Although an internal ribosome entry site (*Ires*)-diphtheria toxin (DT) receptor (*Dtr*)-enhanced green fluorescent protein (*Egfp*) cassette was inserted into the 3′ untranslated region of the *Siglech* gene in *Siglech*$^{dtr/dtr}$ mice, EGFP was not expressed in microglia in any CNS region due to unknown mechanisms (data not shown). This is consistent with the lack of EGFP expression in pDCs described in our previous study (Takagi et al., 2011). *C-C chemokine receptor type 2* (*Ccr2*)$^{RFP/RFP}$ knock-in mice on a C57BL/6J background were obtained from The Jackson Laboratory (stock number: 017586) (Saederup et al., 2010). Embryonic day (E)17, and male postnatal day (P)0, 7, 14, 28, and 8-12-week-old (W) (adult) mice were used. This study was approved by the local animal ethics committee of Nagoya University (approval numbers: 25107, 26181, 27204 and 28303). All experimental procedures were conducted in accordance with standard guidelines for animal experiments from the Nagoya University Graduate School of Medicine, the Animal Protection and Management Law of Japan (No. 105), and the Ethical Issues of the International Association for the Study of Pain (Zimmermann, 1983). All efforts were made to minimize the number of animals used and their suffering.

Injury models

Adult mice were anesthetized with isoflurane or pentobarbital for surgery. The optic nerve of *Ccr2*$^{RFP/+}$ mice was crushed at ~1 mm from the optic disc for 5 seconds using fine forceps, and analyzed by immunohistochemistry 7 days after injury. Experimental autoimmune encephalomyelitis (EAE) was induced by immunizing *Ccr2*$^{RFP/+}$ mice with $MOG_{35–55}$ peptide followed by injection of pertussis toxin as previously described (Bando et al., 2015). After the appearance of hindlimb paralysis, the ventral white matter of the L4 spinal cord was analyzed by immunohistochemistry. The sciatic nerve was unilaterally transected using scissors and, 7 days after surgery, the sciatic nerve and spinal dorsal horn were analyzed by immunohistochemistry and quantitative real-time PCR (qPCR). For a neuropathic pain model, the spinal L4 nerve of WT and *Siglech*$^{dtr/dtr}$ mice was unilaterally transected using scissors according to our method described previously (Kobayashi et al., 2016), and pain testing, immunohistochemistry and qRT-PCR were performed 1, 3, 7 and 14 days after surgery.

Ablation of microglia

DT (50 μg/kg) (Sigma Aldrich) was intraperitoneally administrated to P7 or adult *Siglech*$^{dtr/dtr}$ mice. For the nerve-injury model, the sciatic nerve of adult *Siglech*$^{dtr/dtr}$ mice was unilaterally transected 7 days before DT administration. Brains, spinal cords and sciatic nerves were processed for immunohistochemistry 2 days after DT administration.

Immunohistochemistry

Immunohistochemistry was performed according to our previously described method with slight modification (Konishi et al., 2007). Mice were perfused with Zamboni's fixative (0.1 M phosphate buffer containing 2% paraformaldehyde and 0.2% picric acid), and then brains, the L4 level of spinal cords, optic and sciatic nerves were dissected. Post-fixation was avoided in this study because over-fixation significantly decreased the immunoreactivity of Siglec-H. The brains of E17 mice and spinal cords of adult EAE model mice were fixed by immersion in Zamboni's fixative for 4–6 h at 4°C. Tissues were dehydrated in 25% sucrose in 0.1 M phosphate buffer overnight at 4°C and then frozen in dry ice. Floating or slide-mounted sections were cut on a microtome at 16 or 30 μm, washed in 0.01 M phosphate buffered saline (PBS), and then reacted with primary antibodies diluted in a blocking solution (0.01 M PBS containing 1% bovine serum albumin, 0.1% Triton X100 and 0.1% NaN_3). The following primary antibodies were used: rabbit polyclonal anti-Iba1 (WAKO #019-19741, RRID: AB_839504), goat polyclonal anti-Iba1 (Abcam #ab5076, RRID: AB_2224402), rat monoclonal anti-CD206 (Bio-rad #MCA2235GA, RRID: AB_322613), goat polyclonal anti-CD206 (R&D systems #AF2535, RRID: AB_2063012), rabbit polyclonal anti-laminin (Abcam #ab11575, RRID: AB_298179), and rabbit polyclonal anti-protein kinase C gamma (PKCγ) (Santa Cruz Biotechnology #sc-211, RRID: AB_632234). Characterization of the polyclonal anti-Siglec-H antibody used in the present study was described in our previous study (Zhang et al., 2006). Briefly, a sheep was immunized with the extracellular domain of mouse Siglec-H fused with Fc region of human IgG (Fc) (Siglec-H-Fc), and anti-Siglec-H antibody was purified by affinity chromatography using Siglec-H-Fc-coupled column. For antigen absorption tests, anti-Siglec-H antibody was reacted with 1.0 μM of the Fc, Siglec-H-Fc or Siglec-E-Fc (Biolegend) in 0.01M PBS overnight at 4°C. The reaction mixture was centrifuged at 10,000g for 20 min at 4°C, and then the supernatant was used as the primary antibody solution. After reaction with primary antibodies, sections were washed in 0.01 M PBS, and reacted with secondary antibodies conjugated with Alexa Fluor 488, 594 or 647 (Thermo Fisher Scientific). After washing in 0.01 M PBS, sections were mounted with FluorSave reagent (Merck Millipore). Images were taken using an FV10i confocal microscope (Olympus).

Quantitative histological analysis

Rate of Siglec-H$^+$ microglia in the cerebral cortex: In adult mice, we defined parenchymal Iba1$^+$ cells with ramified morphology as microglia, and quantified the rate of Siglec-H$^+$ microglia in the cerebral cortex, corpus callosum, hippocampal CA1 area, ventral posterolateral/posteromedial thalamic nucleus, cerebellar cortex, spinal trigeminal nucleus of the medulla, and the dorsal horn of the spinal cord in Iba1 stained sections. In contrast to adult mice, microglia were not fully ramified in embryonic and early postnatal mice, and could not be clearly distinguished from pvMΦ by Iba1 immunostaining. We therefore calculated the Siglec-H$^+$ rate against all Iba1$^+$ cells in the cerebral cortex under the meninges in E17, P0 and P7 mice. A total of 36 images (3 fields/section, 3 sections/animal, 4 animals) were analyzed.

Rate of Siglec-H$^+$ pvMΦ or mMΦ in the cerebral cortex: We calculated the Siglec-H$^+$ rate of CD206$^+$ pvMΦ or mMΦ in the cerebral cortex of adult mice. A total of 36 images (3 fields/section, 3 sections/animal, 4 animals) were analyzed.

Rate of Siglec-H$^+$ microglia and circumventricular organ MΦ (cvoMΦ) in the area postrema: We calculated the Siglec-H$^+$ rate of Iba1$^+$/CD206$^-$ microglia or cvoMΦ in the area postrema of adult mice. A total of 12 images (1 field/section, 3 sections/animal, 4 animals) were analyzed.

Percentage of three different populations of Iba1$^+$ cells in the choroid plexus: We calculated the percentage of Siglec-H$^+$/CD206$^-$, Siglec-H$^-$/CD206$^+$ and Siglec-H$^+$/CD206$^+$ cells against total Iba1$^+$ cells in the choroid plexus of lateral ventricle of adult mice. A total of 12 images (1 field/section, 3 sections/animal, 4 animals) were analyzed.

Rate of Siglec-H$^+$ monocytes in the EAE model: The ventral white matter of the L4 spinal cord in *Ccr2*$^{RFP/+}$ mice with EAE was analyzed. Sections were stained with anti-Siglec-H antibody, and the Siglec-H$^+$ rate in RFP$^+$ infiltrating monocytes was calculated. A total of 45 images (3 fields/section, 3 sections/animal, 5 animals) were analyzed.

Rate of microglia and MΦ ablation: Sections were prepared form the cerebral cortex and medulla (for the area postrema) of non-injured adult *Siglech*$^{dtr/dtr}$ mice 2 days after DT administration, and double-stained with anti-Iba1 and anti-CD206 antibodies. We defined Iba1$^+$/CD206$^-$ and Iba1$^+$/CD206$^+$ cells as microglia and MΦ, respectively, and counted cell numbers in 12 images (1 field/section, 4 sections/animal, 3 animals). For the nerve injury model, sections of L4 spinal cord dorsal horn and sciatic nerve were prepared from sciatic nerve-injured adult *Siglech*$^{dtr/dtr}$ mice 2 days after DT administration. Spinal sections were immunoreacted with anti-Iba1 and anti-PKCγ antibodies to stain microglia and the inner lamina II of the dorsal horn (Malmberg, Chen, Tonegawa, & Basbaum, 1997), respectively. The number of Iba1$^+$ cells in lamina I and outer lamina II (I/IIo) was counted and is shown as microglial numbers because pvMΦ were rare and their numbers were negligible in the dorsal horn. The sciatic nerve was stained with anti-Iba1 antibody to identify monocytes/MΦ. Images taken by a

confocal microscope were acquired using the same laser power and sensitivity, and Iba1$^+$ areas were measured using Image J software version 10.2 (NIH, RRID: SCR_003070). A total of 12 images (1 field/section, 4 sections/animal, 3 animals) were analyzed. For developmental stages, DT was administrated to P7 *Siglech*$^{dtr/dtr}$ mice. Sections of the cerebral cortex were prepared after 2 days, and were stained with anti-Iba1 antibody. CD206 immunostaining was not performed because pvMΦ and mMΦ could not be distinguished from microglia by CD206 immunoreactivity. We counted the number of Iba1$^+$ cells in the cerebral cortex beneath the meninges in a total of 12 images (1 field/section, 4 sections/animal, 3 animals).

Number of microglia in the dorsal horn of the neuropathic pain model: Adult WT and *Siglech*$^{dtr/dtr}$ L4 spinal cord sections were prepared 7 days after L4 nerve transection. Sections were stained with anti-Iba1 and anti-PKCγ antibodies, and the number of Iba1$^+$ cells in the lamina I/IIo of the dorsal horn was counted. A total of 16 images (1 field/section, 4 sections/animal, 4 animals) were analyzed.

qPCR

Cerebral cortex was collected from E17, P0, P7, P14, P28 and 8W WT, and 8W *Siglech*$^{dtr/dtr}$ mice (n = 3). L4 spinal dorsal horn and sciatic nerve were taken from WT mice 7 days after sciatic nerve transection (n = 3). L4 spinal dorsal horn was dissected from WT and *Siglech*$^{dtr/dtr}$ mice, 0 (naive), 1, 3, 7 and 14 days after L4 nerve transection (n = 3). mRNA was purified from tissues using the acid guanidine iso-thiocyanate/phenol/chloroform extraction method, and converted to cDNA by SuperScript III (Thermo Fisher Scientific). qPCR was performed using StepOnePlus (Applied Biosystems) with Fast SYBR Green Master Mix (Applied Biosystems): 1 cycle of 95°C for 20 s, 40 cycles of 95°C for 3 s, and 60°C for 30 s. Primers were as follows; *glyceraldehyde-3-phosphate dehydrogenase* (*Gapdh*) (sense 5′-TGACGTGCCGCCTGGAGAAA-3′, antisense 5′-AGTGTAGCCCAAGATGCCCTTCAG-3′), *Siglech* (sense 5′-TGGTACAGGTAGCCATGGGA-3′, antisense 5′-TGTGTTGCTGGTCTCTCCAC-3′), *allograft inflammatory factor 1* (*Aif1*) (gene encoding Iba1) (sense 5′-GGATCTGCCGTCCAAAC-3′, antisense 5′-GCATTCGCTTCAAGGACA-3′), *tumor necrosis factor (TNF)-α* (*Tnfa*) (sense 5′-GTGGAACTGGCAGAAGAGGC-3′, antisense 5′-AGACAGAAGAGCGTGGTGGC-3′), *interleukin (IL)-1β* (*Il1b*) (sense 5′-CTGTGTCTTTCCCGTGGACC-3′, antisense 5′-CAGCTCATATGGGTCCGACA-3′), *Il10* (sense 5′-GGTTGCCAAGCCTTATCGGA-3′, antisense 5′-ACCTGCTCCACTGCCTTGCT-3′), and *transforming growth factor* (*TGF*)*-β1* (*Tgfb1*) (sense 5′-CCGCAACAACGCCATCTATG-3′, antisense 5′-TGCCGTACAACTCCAGTGAC-3′). Amplified PCR samples were subjected to melting analysis to confirm amplicon specificity.

Results were normalized to *Gapdh* and analyzed using the 2−ΔCt method.

Behavioral analysis of neuropathic pain

WT and *Siglech*$^{dtr/dtr}$ mice, 0, 3, 7 and 14 days post L4 spinal nerve transection were analyzed (n = 4). Mice were individually placed in an opaque chamber with a wire mesh floor. After habituation at least for 30 min, the tip of an Electronic von Frey Anesthesiometer (IITC Life Science) was applied to the plantar surfaces of their hindpaws and the paw withdrawal threshold (PWT) was measured.

Statistical analysis

All values are expressed as the mean ± S.E.M. Changes in gene expression and cell numbers were analyzed with the unpaired Student's *t*-test. PWT data was analyzed by two-way ANOVA with a *post hoc* Bonferroni test. $p < 0.05$ was considered statistically significant.

Results

Siglec-H is specifically expressed by microglia in the steady state CNS of adult mice, except for in the choroid plexus

We stained sections of cerebral cortex prepared from adult mice with a polyclonal antibody against Siglec-H (Figure 1) (Zhang et al., 2006). Clear signals were observed in Iba1$^+$ microglia with ramified morphologies in the parenchyma (Figure 1a–c). The signals disappeared after absorption of the antibody with antigen (Siglec-H-Fc) (Figure 1d–f), suggesting the antibody-antigen specificity. Because Siglec-E was also shown as a microglial signature gene among Siglec family members in mice (Bennett et al., 2016; Claude et al., 2013; Hickman et al., 2013), we confirmed that the Siglec-H antibody did not cross-react with Siglec-E (Figure 1g–i). The antibody-antigen specificity was further confirmed using *Siglech* knock-down mice. In *Siglech*$^{dtr/dtr}$ mice, an *Ires* and the gene encoding the DT receptor were knocked into the 3′ untranslated region of the *Siglech* gene (Takagi et al., 2016; Takagi et al., 2011). This genetic modification was not expected to affect the expression of *Siglech*; however, our previous study found that Siglec-H expression was knocked-down in pDCs in the immune system of *Siglech*$^{dtr/dtr}$ mice. qPCR showed that levels of *Siglech* mRNA were knocked-down in the cerebral cortex of *Siglech*$^{dtr/dtr}$ mice (75.1% decrease compared with WT by qPCR, $n = 3$, $p < 5.0 \times 10^{-6}$). In line with the downregulation of mRNA, microglial Siglec-H immunoreactivity was significantly lower in *Siglech*$^{dtr/dtr}$ mice compared with WT (Figure 1j–o), demonstrating antibody-antigen specificity of the Siglec-H antibody in immunohistochemistry.

In cortical sections, CD206$^+$ pvMΦ were found along medium- or large-sized vessels but not along capillaries (single arrowheads in Figure 2b), and CD206$^+$ mMΦ were found in the meninges (double arrowheads in Figure 2b) (Galea et al., 2005; Goldmann et al., 2016). These two types of macrophages had spindle or round shapes with fewer processes compared with parenchymal microglia (Figure 2b) and were almost negative for Siglec-H (Figure 2a; Siglec-H$^+$ pvMΦ: 1.7 ± 0.6%; Siglec-H$^+$ mMΦ: 0.3 ± 0.3%), whereas parenchymal ramified microglia were positive in the same sections (arrows in Figure 2a). In contrast to the microglia-specific expression of Siglec-H, Iba1 was expressed by all myeloid cells in cortical sections (Siglec-H$^+$ microglia, CD206$^+$ pvMΦ and CD206$^+$ mMΦ) (Figure 2e–h). Circumventricular organs are brain areas lacking the blood–brain barrier (Kaur & Ling, 2017; Morita & Miyata, 2012). Sensory circumventricular organs, such as the ‘area postrema’ in the dorsal medulla, contain a large number of MΦ around capillaries (Goehler, Erisir, & Gaykema, 2006; Murabe, Nishida, & Sano, 1981; Willis, Garwood, & Ray, 2007). We defined MΦ within circumventricular organs as circumventricular organ MΦ (cvoMΦ) in this study because cvoMΦ are different from pvMΦ in that cvoMΦ contact capillaries and are assumed to play specific roles, such as forming a size-selective diffusion barrier around capillaries in circumventricular organs (Goehler, Erisir, &

Gaykema, 2006; Murabe, Nishida, & Sano, 1981; Willis, Garwood, & Ray, 2007). In the area postrema, Siglec-H was not detected in Iba1$^+$/CD206$^+$ cvoMΦ with few processes (arrowheads in the inset of Figure 2i–l); however, Siglec-H was expressed by putative Iba1$^+$/CD206$^-$ microglia with ramified shapes (an arrow in the inset of Figure 2i–l; Siglec-H$^+$ rate of Iba1$^+$/CD206$^-$ cells: 96.4 ± 0.9%), except for a minor Iba1$^+$ population that expressed both Siglec-H and CD206 (an asterisk in Figure 2i–l; 3.6 ± 0.9% of Iba1$^+$/Siglec-H$^+$ cells; 3.2 ± 0.7% of Iba1$^+$/CD206$^+$ cvoMΦ). We obtained the same results in another sensory circumventricular organ, the 'subfornical organ' at the roof of the third ventricle (data not shown). In contrast to the cerebral cortex and sensory circumventricular organs, results were different in the choroid plexus (Figure 2m–p), which is known to contain cpMΦ with a higher turnover rate compared with mMΦ and pvMΦ (Goldmann et al., 2016). In addition to Siglec-H$^+$/CD206$^-$ (an arrow in Figure 2m–p; 17.5 ± 3.0% of total Iba1$^+$ cells) and Siglec-H$^-$/CD206$^+$ cells (arrowheads in Figure 2m–p; 60.3 ± 4.5% of total Iba1$^+$ cells), Siglec-H$^+$/CD206$^+$ cells were also frequently observed (asterisks in Figure 2m–p; 11.5 ± 2.0% of total Iba1$^+$ cells; 40.0 ± 6.3% of Iba1$^+$/Siglec-H$^+$ cells; 16.2 ± 2.7% of Iba1$^+$/CD206$^+$ cells).

Microglia-specific Siglec-H expression was also examined in the parenchyma of representative CNS regions, including hippocampal CA1 (Supporting Information Figure S1a–c) and the white matter (corpus callosum) (Supporting Information Figure S1d–f). The rate of Siglec-H$^+$ microglia with respect to Iba1$^+$ cells with ramified morphologies in the parenchyma was almost 100% in all regions examined (cerebral cortex: 100.0%; corpus callosum: 100.0%; hippocampus: 99.7 ± 0.3%; thalamus: 100.0%; cerebellum: 99.8 ± 0.2%; medulla: 100.0%; spinal cord: 100.0%) (Supporting Information Figure S1g), and all Siglec-H$^+$ cells were Iba1$^+$. These results demonstrated that Siglec-H expression was confined to microglia in the steady state CNS except for in the choroid plexus.

Siglec-H is specifically expressed by microglia in the developing CNS

The recently identified microglia-specific markers, TMEM119 and Sall1, are not specific during mouse development (Bennett et al., 2016; Buttgereit et al., 2016; Harrison, Nishinakamura, Jones, & Monaghan, 2012); therefore, we tested whether Siglec-H is specific for microglia during development (Figure 3). Even though microglial numbers in the cerebral cortex were small at E17 (Swinnen et al., 2013), *Siglech* mRNA was clearly detected by qPCR at a similar level to *Aif1* mRNA (encoding Iba1) (Figure 3a). Because microglia express Iba1 from an early developmental stage (Hirasawa et al., 2005), we expected that Siglec-H immunoreactivity could be detected in embryonic microglia by immunohistochemistry. In embryonic mice, it was difficult to immunohistochemically distinguish microglia from mMΦ or pvMΦ, because immature microglia also expressed CD206 (data not shown) and were not fully

ramified. Although microglia could not be defined clearly by morphology at E17, Siglec-H expression was observed in putative Iba1$^+$ microglia in parenchyma, but not in some Iba1$^+$ cells in the meninges, which might correspond to mMΦ (Figure 3b–d). At P7, microglial ramification proceeded and microglia were distinguishable from mMΦ and pvMΦ by their morphologies (Figure 3f). Siglec-H was detected in ramified microglia in parenchyma whereas putative mMΦ, which had large cell bodies with few processes, were negative for Siglec-H (Figure 3e–g). A quantitative study showed that Siglec-H was expressed by most Iba1$^+$ cells during development (E17: 96.4 ± 0.6%; P0: 95.5 ± 0.7%; P7: 98.5 ± 1.0%; relative to all Iba1$^+$ cells in the cerebral cortex beneath the meninges) (Figure 3h).

Siglec-H is not expressed by monocytes infiltrating an injured or inflamed nervous system

Circulating CCR2$^+$ monocytes can enter the nervous system upon neuronal injury or inflammation, and play distinct roles from those of microglia (King, Dickendesher, & Segal, 2009; Mildner et al., 2009; Varvel et al., 2016; Yamasaki et al., 2014). We hypothesized that Siglec-H expression could discriminate resident microglia from infiltrating monocytes, and examined the possibility using an optic nerve injury model (Figure 4a–h). We used *Ccr2*$^{RFP/+}$ mice, in which monocytes infiltrating the CNS are labeled with red fluorescent protein (RFP) (Saederup et al., 2010). Siglec-H expression was observed in Iba1$^+$ microglia with elongated morphology along the axons of the control optic nerve, and no RFP$^+$ monocytes were found (Figure 4a–d). In contrast, a significant number of RFP$^+$ monocytes with a round or spindle shape had invaded the injured optic nerve 7 days after crush injury (Figure 4f), and these RFP$^+$ monocytes were negative for Siglec-H (Figure 4e–h). We could not perform a quantitative study of Siglec-H$^+$ monocytes because the monocyte density was high and counting monocyte numbers was difficult (Figure 4f).

We also tested an inflammatory model of the CNS (Figure 4i–p). We immunized *Ccr2*$^{RFP/+}$ mice with MOG peptide to induce EAE. After hindlimb paralysis appeared, the spinal cord was dissected and processed for immunohistochemistry. In contrast to control mice (Figure 4j), RFP$^+$ monocytes with round or spindle shapes were infiltrated into the white matter of mice with EAE (Figure 4n). While activated Iba1$^+$ microglia with hypertrophic morphology expressed Siglec-H, infiltrating monocytes were negative for Siglec-H (Figure 4m–p), except for a minor population that markedly expressed Siglec-H compared with resident microglia (an asterisk in Figure 4m–p; 1.8 ± 0.3% of total RFP$^+$ cells).

In addition to the CNS, we examined the PNS. Peripheral nerve injury causes accumulation of MΦ in the distal part of the injured nerve, which is necessary for Wallerian degeneration (Chen, Piao, & Bonaldo, 2015). Although resident MΦ in peripheral nerves proliferate and contribute to the pool, the main source of accumulated MΦ is monocytes

recruited from the circulation (Beuche & Friede, 1984). Thus we examined whether monocytes infiltrating the injured peripheral nerve express Siglec-H (Figure 5). The nerve injury caused accumulation of microglia and monocytes/MΦ in the ipsilateral spinal cord (Figure 5b,e) and injured nerve (Figure 5h), respectively, 7 days after sciatic nerve transection. Although Siglec-H was expressed by Iba1^{+}-activated microglia in the dorsal horn (Figure 5a–f), Siglec-H expression was not detected in Iba1^{+} monocytes/MΦ in the injured sciatic nerve (Figure 5g–i). These histological data were confirmed by qPCR (Figure 5j,k). Siglec-H expression was increased concomitantly with Iba1 induction in the dorsal horn after injury (Figure 5j). In contrast, Siglec-H expression was not induced in the injured nerve although Iba1 expression was markedly increased (Figure 5k).

Collectively, Siglec-H can be used as a histological marker that distinguishes resident microglia from infiltrating monocytes both in the CNS and PNS, except for a minor population.

The *Siglech* locus is suitable for microglia-specific gene targeting

Our histological analyses indicated Siglec-H to be a microglia-specific marker in the nervous system, which prompted us to explore the suitability of the *Siglech* locus for microglia-specific gene targeting in mice (Figure 6). To this end, we used *Siglech*$^{dtr/dtr}$ mice, in which Siglec-H^{+} cells express the DT receptor and can be ablated by systemic DT administration (Takagi et al., 2011). After peritoneal injection of DT into adult *Siglech*$^{dtr/dtr}$ mice, a significant number of microglia in the cerebral cortex was ablated within 2 days (Figure 6a,b). The number of Iba1^{+}/CD206^{-} microglia decreased to 20.6% (Figure 6c), while those of CD206^{+} pvMΦ and mMΦ were unchanged (Figure 6d,e). We also demonstrated in the area postrema that DT was ineffective at ablating CD206^{+} cvoMΦ in contrast to Iba1^{+}/CD206^{-} microglia (85.8% decrease in DT-administrated group) (Figure 6f–i).

We also demonstrated that *Siglech* locus-mediated gene targeting had no effects on infiltrating monocytes. We prepared adult *Siglech*$^{dtr/dtr}$ mice with sciatic nerve injury and 7 days after surgery DT was administered to the mice and cell ablation rates calculated (Figure 6j–o). For microglia in the dorsal horn, we counted the number of parenchymal Iba1^{+} cells without CD206 staining because pvMΦ were rare and their number was negligible in the dorsal horn. In lamina I and outer II (I/IIo) of the dorsal horn, which was defined by visualizing inner lamina II by PKCγ immunostaining (Malmberg, Chen, Tonegawa, & Basbaum, 1997), microglial numbers were significantly reduced both in the contralateral and ipsilateral side, 2 days after DT administration (contralateral side: 76.6% decrease in DT-administrated group; ipsilateral side: 78.9% decrease in DT-administrated group) (Fig. 6j–l). By contrast, the number of monocytes/MΦ in the sciatic nerve was unchanged (Figure 6m–o). Taken together, these results indicate that the *Siglech* locus is suitable for microglia-specific gene targeting in adult mice

without affecting the behavior of CNS-associated MΦ, such as pvMΦ, mMΦ and cvoMΦ, and infiltrating monocytes in the nervous system.

A hallmark of Siglec-H was its expression in immature microglia (Figure 3); therefore, we administrated DT to P7 *Siglech*$^{dtr/dtr}$ mice and analyzed the cerebral cortex at P9 (Figure 6p–r). Similar to E17 (Figure 3b–d) and P7 (Figure 3e–g) mice, pvMΦ and mMΦ could not be distinguished from microglia by CD206 immunoreactivity at P9 (data not shown). Thus we stained laminin to visualize vessels and meninges (Figure 6p,q). Most Iba1^{+} ramified microglia were ablated within 2 days of DT administration. In contrast, Iba1^{+} cells with large cell bodies and few processes, located in the perivascular region (putative pvMΦ indicated by single arrowheads in Figure 6p,q) and meninges (putative mMΦ indicated by double arrowheads in Figure 6p,q), were unaffected. Statistical analysis showed a 91.9% decrease of Iba1^{+} cells in the cerebral cortex beneath the meninges in the DT-administrated group (Figure 6r). It should be noted that most of the remaining Iba1^{+} cells (8.1%) were putative pvMΦ along the vessels, and that almost all the microglia were ablated in the parenchyma.

Siglec-H suppressed inflammatory responses of activated microglia

Finally we addressed Siglec-H function using a mouse neuropathic pain model. In this model, transection of the L4 spinal nerve induces microglial activation in the L4 dorsal horn, and the resulting inflammatory responses of activated microglia develop and prolong neuropathic pain (Tsuda, 2016). In the ipsilateral dorsal horn of the model mice, expression of *Siglech* mRNA increased after injury with a peak at 3 days (Figure 7a), when the microglial numbers also reached a peak (Kobayashi et al., 2016). *Siglech* mRNA was significantly decreased in the ipsilateral dorsal horn of *Siglech*$^{dtr/dtr}$ mice compared with WT (Figure 7a). Immunohistochemistry demonstrated that Siglec-H protein was expressed in activated Iba1^{+} microglia in the ipsilateral dorsal horn of WT mice (Figure 7b–g). However, Siglec-H immunoreactivity was very low in *Siglech*$^{dtr/dtr}$ mice (Figure 7h–j). Thus we assumed that Siglec-H could be functionally impaired in *Siglech*$^{dtr/dtr}$ mice, and we analyzed the functional consequences of *Siglech* impairment in the pain model. qPCR showed that the nerve injury induced the expression of representative pro-inflammatory cytokines, *Tnfa* and *Il1b*, in the ipsilateral dorsal horn (Figure 7k) (Tsuda, 2016). *Siglech* knock-down increased the expression of *Tnfa* and *Il1b* but did not affect expression of anti-inflammatory cytokines, such as *Il10* and *Tgfb1*. Because the ipsilateral dorsal horn of WT and *Siglech*$^{dtr/dtr}$ mice contained almost equal numbers of microglia (1.03-fold increase in *Siglech*$^{dtr/dtr}$ compared with WT mice at 7 days) (Figure 7l–n), the increase in *Tnfa* and *Il1b* mRNA observed in *Siglech*$^{dtr/dtr}$ mice was likely the result of upregulation of gene expression in microglia. Lastly, we evaluated mechanical allodynia in *Siglech*$^{dtr/dtr}$ mice using the von Frey test (Figure 7o,p). Although PWT of the

contralateral side was comparable between WT and *Siglech*$^{dtr/dtr}$ mice (Figure 7o), that of the ipsilateral side was lower in *Siglech*$^{dtr/dtr}$ mice after nerve injury with significant differences at day 3 (Figure 7p), demonstrating that mechanical allodynia was exacerbated in *Siglech*$^{dtr/dtr}$ mice. These results suggest that Siglec-H suppresses the pro-inflammatory response of microglia, reducing neuropathic pain.

Discussion

In this study, we explored the feasibility of Siglec-H as a specific marker for microglia in the nervous system. We revealed that almost all microglia in the CNS parenchyma expressed Siglec-H, from developmental to mature stages (Figures 1–3; Supporting Information Figure S1), and the expression was maintained in activated microglia after CNS (Figure 4) and PNS injuries (Figures 5 and 7a–g). In contrast, Siglec-H expression was largely absent from other myeloid cells in the nervous system: CNS-associated MΦ (pvMΦ, mMΦ and cvoMΦ; Figure 2), and monocytes infiltrating into the CNS (Figure 4) and PNS (Figure 5). On the basis of the Siglec-H expression profile, we further demonstrated the use of the *Siglech* locus for microglia-specific gene manipulation in both mature and developing mice (Figure 6). Collectively, we conclude that Siglec-H is a specific marker that will be highly useful for microglial studies.

Siglec-H is a single-pass transmembrane protein belonging to the CD33-related Siglec family (Macauley, Crocker, & Paulson, 2014). Although there are no clear orthologs in human, Siglec-L2 is ~42% homologous and is assumed to be a potential ortholog (Zhang et al., 2006). Siglec-H is known as a marker for pDCs in the immune system (Blasius et al., 2006; Takagi et al., 2011; Zhang et al., 2006). Several previous studies employing transcriptome or flow cytometric analyses using isolated cells suggested that Siglec-H was abundantly expressed in microglia compared with peripheral myeloid cells, such as circulating monocytes and peripheral MΦ (Bedard, Tremblay, Chernomoretz, & Vallieres, 2007; Butovsky et al., 2014; Chiu et al., 2013; Gautier et al., 2012; Hickman et al., 2013). However, no immunohistochemical studies were performed in the nervous system, and it remained unknown whether Siglec-H was expressed by CNS-associated MΦ as well as monocytes infiltrating in the nervous system. In this study, we demonstrated that Siglec-H expression was largely confined to microglia (Figures 1–5; Supporting Information Figure S1) by using a Siglec-H-specific antibody (Zhang et al., 2006), whose antigen-specificity was confirmed by an absorption test (Figure 1d–i) and by the use of *Siglech* knock-down mice (Figures 1m–o and 7h–j). Several marker antibodies such as Iba1 and CD11b are frequently used for immunohistochemical detection of microglia; however, these molecules are also expressed by CNS-associated MΦ in the steady state (Figure 2) as well as by infiltrating monocytes in the injured nervous system (Figure 4e–h and 5g–i) (Greter, Lelios, & Croxford, 2015; Prinz & Priller, 2014; Prinz, Priller, Sisodia, & Ransohoff, 2011). This broader expression makes it difficult to discriminate microglia from other myeloid cells by immunohistochemistry. In addition to these classical markers, Bennette et al. (Bennett et al., 2016) recently reported a transmembrane protein, TMEM119, as a microglia-specific marker, for which mMΦ, pvMΦ and cpMΦ, and CNS-infiltrating monocytes were negative. Although the authors demonstrated specificity of

TMEM119 expression in microglia, the expression was very low or absent in immature microglia in embryonic and early postnatal mice. Sall1 has also recently been shown to be a microglia-specific transcription factor using *Sall1*^{GFP} and *Sall1*^{CreER} knock-in mice (Buttgereit et al., 2016; Koso et al., 2016). Sall1 expression was highly restricted to microglia in the CNS of adult mice; however, Sall1 expression was abundantly observed in neuronal/glial progenitor cells in embryonic mice (Buttgereit et al., 2016; Harrison, Nishinakamura, Jones, & Monaghan, 2012). This is in contrast to Siglec-H because Siglec-H expression was observed in microglia in embryonic and early postnatal mice (Figure 3). More recently, Mildner et al. (Mildner et al., 2017) reported that a purinoceptor, $P2Y_{12}$, is detected in microglia but not in pvMΦ and mMΦ in the developing human brain. Additionally, previous reports showed that $P2Y_{12}$ expression was detected in microglia but not in splenic MΦ or CNS-infiltrating monocytes by immunohistochemistry in mice (Butovsky et al., 2014; Haynes et al., 2006). However, $P2Y_{12}$ expression is significantly decreased or diminished in activated microglia (Amadio et al., 2014; Haynes et al., 2006; Mildner et al., 2017), whereas Siglec-H expression was maintained in microglia activated by CNS (Figure 4) and PNS injuries (Figures 5 and 7b–g).

In addition to microglia, Siglec-H was detected in Iba1$^+$ cells in the choroid plexus (Figure 2m–p). Iba1$^+$ cells in the choroid plexus can be divided into three subsets: Siglec-H$^+$/CD206$^-$ (an arrow in Figure 2m–p), Siglec-H$^-$/CD206$^+$ (arrowheads) and Siglec-H$^+$/CD206$^+$ (asterisks) cells. This suggests that cpMΦ consists of heterogeneous populations in contrast to pvMΦ, mMΦ and cvoMΦ. A recent paper revealed the heterogeneity of cpMΦ (Goldmann et al., 2016). The authors showed that cpMΦ, pvMΦ and mMΦ were all derived from precursors in the yolk sac and/or the fetal liver. However, cpMΦ have a shorter life span and are gradually replenished by circulating myeloid cells, while pvMΦ and mMΦ persist throughout life. Subpopulation(s) of cpMΦ can express some microglial signature genes, which is supported by the presence of $P2Y_{12}^+$ myeloid populations in the choroid plexus of the fetal human brain (Mildner et al., 2017).

In addition to the immunohistochemical reliability of Siglec-H, we addressed the feasibility of using the *Siglech* locus for microglia-specific gene manipulation using *Siglech*$^{dtr/dtr}$ knock-in mice (Figure 6). Genetic targeting of microglia in mice was performed using the gene loci or promoter/enhancer regions of *Itgam* (encoding CD11b), *Csf1r* and *Cx3cr1* (Boillee et al., 2006; Jung et al., 2000; Pfrieger & Slezak, 2012; Sasmono et al., 2003). However, given that these molecules are expressed by a variety of myeloid cells, the effect of the genetic modification will not necessarily be restricted to microglia (Goldmann et al., 2016; Wieghofer, Knobeloch, & Prinz, 2015). To circumvent this problem, a new system was established based on the longevity of microglia (Goldmann et al., 2013; Parkhurst et al., 2013). When *Cx3cr1*$^{CreER/+}$ mice are crossed to mice harboring a floxed allele, both microglia and peripheral Cx3CR1$^+$ cells,

including monocytes, undergo recombination upon tamoxifen administration. After an interval of several weeks, microglial recombination persists whereas peripheral Cx3CR1^{+} cells are replaced by bone marrow-derived progenitors without recombination. Even with this technique, recombination of mMΦ and pvMΦ can be maintained for a long period together with microglia because mMΦ and pvMΦ are long-lived cells (Goldmann et al., 2016). Thus finding a microglia-specific gene locus is considered important. Results from the present cell ablation study suggest the usefulness of the *Siglech* locus for microglia-specific targeting in the CNS (Figure 6a–l and p–r). Another advantage of using the *Siglech* locus is a lack of recombination in PNS-infiltrating monocytes (Figure 6j–o). The present results suggest that a *Siglech*^{Cre} mouse would be a beneficial tool for future microglial studies.

A previous study using cultured microglia suggested that Siglec-H was a phagocytic receptor for glioma cells (Kopatz et al., 2013). This is the only report addressing the role of Siglec-H in microglia, and Siglec-H functions in the nervous system, especially *in vivo*, remain elusive. In the immune system, an anti-inflammatory role of Siglec-H in pDCs has been proposed (Blasius et al., 2006; Puttur et al., 2013; Takagi et al., 2016; Takagi et al., 2011). Therefore, we tested the possibility that Siglec-H also suppressed pro-inflammatory responses of microglia using a mouse neuropathic pain model (Tsuda, 2016). We found that *Siglech* knock-down promoted induction of representative pro-inflammatory cytokines in spinal microglia (Figure 7k) without affecting microglial proliferation (Figure 7l–n). We further revealed that pain behavior was exacerbated in *Siglech* knock-down mice (Figure 7o,p). Taken together, Siglec-H-mediated signals appeared to act as a suppressor of pro-inflammatory responses in activated microglia. Siglec-H is proposed to be a cell surface receptor, although ligand(s) remain unidentified (Blasius et al., 2006; Kopatz et al., 2013; Zhang et al., 2006). The intracellular domain of Siglec-H is very short and Siglec-H is known to form a complex with a transmembrane adaptor protein, DNAX-activating protein of 12 kDa (DAP12), to induce intracellular signals (Blasius et al., 2006). In parallel with Siglec-H, other transmembrane receptors with short intracellular domains, such as triggering receptor expressed on myeloid cells 2 (TREM2), also bind to DAP12 for signal-transduction (Bouchon, Hernandez-Munain, Cella, & Colonna, 2001). We recently revealed that TREM2-mediated signals promoted pro-inflammatory responses of microglia via DAP12 in the ipsilateral dorsal horn and exacerbated neuropathic pain (Kobayashi et al., 2016). Both Siglec-H and TREM2 are able to make complexes with DAP12 on microglial surfaces. However, TREM2 promotes inflammation whereas Siglec-H suppresses inflammation. This controversy is also reported in the immune system (Blasius & Colonna, 2006; Linnartz-Gerlach, Kopatz, & Neumann, 2014; Turnbull & Colonna, 2007). Siglec-H and TREM2 are likely to work as an opposing switch for microglial activation via DAP12. Besides neuropathic pain, TREM2/DAP12-mediated microglial

activation is also pivotal for pathogenesis of Alzheimer's disease both in humans and in mouse models of the disease (Guerreiro et al., 2013; Jonsson et al., 2013; Paloneva et al., 2000; Paloneva et al., 2002; Wang et al., 2015; Zhang et al., 2013). Therefore, further studies, such as identification of Siglec-H ligand(s), are needed to reveal the precise molecular mechanisms regulating microglial activity via DAP12.

In conclusion, Siglec-H, together with TMEM119, Sall1 and $P2Y_{12}$, will be useful as "contemporary" markers of mouse microglia throughout developmental, adult and aging stages, in both healthy and injury conditions.

Acknowledgments

All authors have no conflict of interest (COI) to declare. This work was partly supported by KAKENHI (Grants-in-Aid for Scientific Research on Priority Areas “Brain Environment” 231111007 and “Grant-in-Aid for Scientific Research (B)” 16H05117 to H. Kiyama, and “Grants-in-Aid for Young Scientist (B)” 25830050 and “Grant-in-Aid for Scientific Research (C)” 16K07055 to H. Konishi) from the Ministry of Education, Culture, Sports, Science and Technology (MEXT) of Japan, and grants from The Hibino Foundation, The Ichiro Kanehara Foundation and The Hori Sciences and Arts Foundation (all to H. Konishi). We are grateful to Y. Bando (Asahikawa Medical University) for advising EAE model, Y. Itai and M. Okamoto for their technical assistance, and Ms. A. Asano for secretarial works.

References

Ajami, B., Bennett, J. L., Krieger, C., McNagny, K. M., & Rossi, F. M. (2011). Infiltrating monocytes trigger EAE progression, but do not contribute to the resident microglia pool. *Nature Neuroscience*, *14*, 1142-1149.

Amadio, S., Parisi, C., Montilli, C., Carrubba, A. S., Apolloni, S., & Volonte, C. (2014). P2Y(12) receptor on the verge of a neuroinflammatory breakdown. *Mediators of Inflammation*, *2014*, 975849.

Bando, Y., Nomura, T., Bochimoto, H., Murakami, K., Tanaka, T., Watanabe, T., & Yoshida, S. (2015). Abnormal morphology of myelin and axon pathology in murine models of multiple sclerosis. *Neurochemistry International*, *81*, 16-27.

Bedard, A., Tremblay, P., Chernomoretz, A., & Vallieres, L. (2007). Identification of genes preferentially expressed by microglia and upregulated during cuprizone-induced inflammation. *Glia*, *55*, 777-789.

Bennett, M. L., Bennett, F. C., Liddelow, S. A., Ajami, B., Zamanian, J. L., Fernhoff, N. B., . . . Barres, B. A. (2016). New tools for studying microglia in the mouse and human CNS. *Proceedings of the National Academy of Sciences of the United States of America*, *113*, E1738-1746.

Beuche, W. & Friede, R. L. (1984). The role of non-resident cells in Wallerian degeneration. *Journal of Neurocytology*, *13*, 767-796.

Blasius, A. L., Cella, M., Maldonado, J., Takai, T., & Colonna, M. (2006). Siglec-H is an IPC-specific receptor that modulates type I IFN secretion through DAP12. *Blood*, *107*, 2474-2476.

Blasius, A. L. & Colonna, M. (2006). Sampling and signaling in plasmacytoid dendritic cells: the potential roles of Siglec-H. *Trends in Immunology*, *27*, 255-260.

Boillee, S., Yamanaka, K., Lobsiger, C. S., Copeland, N. G., Jenkins, N. A., Kassiotis, G., . . . Cleveland, D. W. (2006). Onset and progression in inherited ALS determined by motor neurons and microglia. *Science*, *312*, 1389-1392.

Bouchon, A., Hernandez-Munain, C., Cella, M., & Colonna, M. (2001). A DAP12-mediated pathway regulates expression of CC chemokine receptor 7 and maturation of human dendritic cells. *Journal of Experimental Medicine*, *194*, 1111-1122.

Butovsky, O., Jedrychowski, M. P., Moore, C. S., Cialic, R., Lanser, A. J., Gabriely, G., . . . Weiner, H. L. (2014). Identification of a unique TGF-beta-dependent molecular and functional signature in microglia. *Nature Neuroscience*, *17*, 131-143.

Buttgereit, A., Lelios, I., Yu, X., Vrohlings, M., Krakoski, N. R., Gautier, E. L., . . . Greter, M. (2016). Sall1 is a transcriptional regulator defining microglia identity and function. *Nature Immunology*, *17*, 1397-1406.

Chen, P., Piao, X., & Bonaldo, P. (2015). Role of macrophages in Wallerian degeneration and axonal regeneration after peripheral nerve injury. *Acta Neuropathologica*, *130*, 605-618.

Chiu, I. M., Morimoto, E. T., Goodarzi, H., Liao, J. T., O'Keeffe, S., Phatnani, H. P., . . . Maniatis, T. (2013). A neurodegeneration-specific gene-expression signature of acutely isolated microglia from an amyotrophic lateral sclerosis mouse model. *Cell Reports*, *4*, 385-401.

Claude, J., Linnartz-Gerlach, B., Kudin, A. P., Kunz, W. S., & Neumann, H. (2013). Microglial CD33-related Siglec-E inhibits neurotoxicity by preventing the phagocytosis-associated oxidative burst. *Journal of Neuroscience*, *33*, 18270-18276.

Galea, I., Palin, K., Newman, T. A., Van Rooijen, N., Perry, V. H., & Boche, D. (2005). Mannose receptor expression specifically reveals perivascular macrophages in normal, injured, and diseased mouse brain. *Glia*, *49*, 375-384.

Gamo, K., Kiryu-Seo, S., Konishi, H., Aoki, S., Matsushima, K., Wada, K., & Kiyama, H. (2008). G-protein-coupled receptor screen reveals a role for chemokine receptor CCR5 in suppressing microglial neurotoxicity. *Journal of Neuroscience*, *28*, 11980-11988.

Gautier, E. L., Shay, T., Miller, J., Greter, M., Jakubzick, C., Ivanov, S., . . . Randolph, G. J. (2012). Gene-expression profiles and transcriptional regulatory pathways that underlie the identity and diversity of mouse tissue macrophages. *Nature Immunology*, *13*, 1118-1128.

Ginhoux, F., Greter, M., Leboeuf, M., Nandi, S., See, P., Gokhan, S., . . . Merad, M. (2010). Fate mapping analysis reveals that adult microglia derive from primitive macrophages. *Science*, *330*, 841-845.

Goehler, L. E., Erisir, A., & Gaykema, R. P. (2006). Neural-immune interface in the rat area postrema. *Neuroscience*, *140*, 1415-1434.

Goldmann, T., Wieghofer, P., Jordao, M. J., Prutek, F., Hagemeyer, N., Frenzel, K., . . . Prinz, M. (2016). Origin, fate and dynamics of macrophages at central nervous system interfaces. *Nature Immunology*, *17*, 797-805.

Goldmann, T., Wieghofer, P., Muller, P. F., Wolf, Y., Varol, D., Yona, S., . . . Prinz, M. (2013). A new type of microglia gene targeting shows TAK1 to be pivotal in CNS autoimmune inflammation. *Nature Neuroscience*, *16*, 1618-1626.

Gomez Perdiguero, E., Klapproth, K., Schulz, C., Busch, K., Azzoni, E., Crozet, L., . . . Rodewald, H. R. (2015). Tissue-resident macrophages originate from yolk-sac-derived erythro-myeloid progenitors. *Nature*, *518*, 547-551.

Greter, M., Lelios, I., & Croxford, A. L. (2015). Microglia Versus Myeloid Cell Nomenclature during Brain Inflammation. *Frontiers in Immunology*, *6*, 249.

Guerreiro, R., Wojtas, A., Bras, J., Carrasquillo, M., Rogaeva, E., Majounie, E., . . . Hardy, J.

(2013). TREM2 variants in Alzheimer's disease. *New England Journal of Medicine*, *368*, 117-127.

Harrison, S. J., Nishinakamura, R., Jones, K. R., & Monaghan, A. P. (2012). Sall1 regulates cortical neurogenesis and laminar fate specification in mice: implications for neural abnormalities in Townes-Brocks syndrome. *Disease Models & Mechanisms*, *5*, 351-365.

Haynes, S. E., Hollopeter, G., Yang, G., Kurpius, D., Dailey, M. E., Gan, W. B., & Julius, D. (2006). The P2Y12 receptor regulates microglial activation by extracellular nucleotides. *Nature Neuroscience*, *9*, 1512-1519.

Hickman, S. E., Kingery, N. D., Ohsumi, T. K., Borowsky, M. L., Wang, L. C., Means, T. K., & El Khoury, J. (2013). The microglial sensome revealed by direct RNA sequencing. *Nature Neuroscience*, *16*, 1896-1905.

Hirasawa, T., Ohsawa, K., Imai, Y., Ondo, Y., Akazawa, C., Uchino, S., & Kohsaka, S. (2005). Visualization of microglia in living tissues using Iba1-EGFP transgenic mice. *Journal of Neuroscience Research*, *81*, 357-362.

Hoeffel, G., Chen, J., Lavin, Y., Low, D., Almeida, F. F., See, P., . . . Ginhoux, F. (2015). C-Myb(+) erythro-myeloid progenitor-derived fetal monocytes give rise to adult tissue-resident macrophages. *Immunity*, *42*, 665-678.

Ito, D., Imai, Y., Ohsawa, K., Nakajima, K., Fukuuchi, Y., & Kohsaka, S. (1998). Microglia-specific localisation of a novel calcium binding protein, Iba1. *Brain Research Molecular Brain Research*, *57*, 1-9.

Jonsson, T., Stefansson, H., Steinberg, S., Jonsdottir, I., Jonsson, P. V., Snaedal, J., . . . Stefansson, K. (2013). Variant of TREM2 associated with the risk of Alzheimer's disease. *New England Journal of Medicine*, *368*, 107-116.

Jung, S., Aliberti, J., Graemmel, P., Sunshine, M. J., Kreutzberg, G. W., Sher, A., & Littman, D. R. (2000). Analysis of fractalkine receptor CX(3)CR1 function by targeted deletion and green fluorescent protein reporter gene insertion. *Molecular and Cellular Biology*, *20*, 4106-4114.

Kaur, C. & Ling, E. A. (2017). The circumventricular organs. *Histology and Histopathology*, 11881.

Kierdorf, K., Erny, D., Goldmann, T., Sander, V., Schulz, C., Perdiguero, E. G., . . . Prinz, M. (2013). Microglia emerge from erythromyeloid precursors via Pu.1- and Irf8-dependent pathways. *Nature Neuroscience*, *16*, 273-280.

King, I. L., Dickendesher, T. L., & Segal, B. M. (2009). Circulating Ly-6C+ myeloid precursors migrate to the CNS and play a pathogenic role during autoimmune demyelinating disease. *Blood*, *113*, 3190-3197.

Kobayashi, M., Konishi, H., Sayo, A., Takai, T., & Kiyama, H. (2016). TREM2/DAP12 Signal Elicits Proinflammatory Response in Microglia and Exacerbates Neuropathic Pain. *Journal of Neuroscience*, *36*, 11138-11150.

Kobayashi, M., Konishi, H., Takai, T., & Kiyama, H. (2015). A DAP12-dependent signal promotes pro-inflammatory polarization in microglia following nerve injury and exacerbates degeneration of injured neurons. *Glia*, *63*, 1073-1082.

Konishi, H., Namikawa, K., & Kiyama, H. (2006). Annexin III implicated in the microglial response to motor nerve injury. *Glia*, *53*, 723-732.

Konishi, H., Namikawa, K., Shikata, K., Kobatake, Y., Tachibana, T., & Kiyama, H. (2007). Identification of peripherin as a Akt substrate in neurons. *Journal of Biological Chemistry*, *282*, 23491-23499.

Kopatz, J., Beutner, C., Welle, K., Bodea, L. G., Reinhardt, J., Claude, J., . . . Neumann, H. (2013). Siglec-h on activated microglia for recognition and engulfment of glioma cells. *Glia*, *61*, 1122-1133.

Koso, H., Tsuhako, A., Lai, C. Y., Baba, Y., Otsu, M., Ueno, K., . . . Watanabe, S. (2016). Conditional rod photoreceptor ablation reveals Sall1 as a microglial marker and regulator of microglial morphology in the retina. *Glia*, *64*, 2005-2024.

Kroner, A., Greenhalgh, A. D., Zarruk, J. G., Passos Dos Santos, R., Gaestel, M., & David, S. (2014). TNF and increased intracellular iron alter macrophage polarization to a detrimental M1 phenotype in the injured spinal cord. *Neuron*, *83*, 1098-1116.

Linnartz-Gerlach, B., Kopatz, J., & Neumann, H. (2014). Siglec functions of microglia. *Glycobiology*, *24*, 794-799.

Macauley, M. S., Crocker, P. R., & Paulson, J. C. (2014). Siglec-mediated regulation of immune cell function in disease. *Nature Reviews Immunology*, *14*, 653-666.

Malmberg, A. B., Chen, C., Tonegawa, S., & Basbaum, A. I. (1997). Preserved acute pain and reduced neuropathic pain in mice lacking PKCgamma. *Science*, *278*, 279-283.

Mildner, A., Huang, H., Radke, J., Stenzel, W., & Priller, J. (2017). P2Y12 receptor is expressed on human microglia under physiological conditions throughout development and is sensitive to neuroinflammatory diseases. *Glia*, *65*, 375-387.

Mildner, A., Mack, M., Schmidt, H., Bruck, W., Djukic, M., Zabel, M. D., . . . Prinz, M. (2009). CCR2+Ly-6Chi monocytes are crucial for the effector phase of autoimmunity in the central nervous system. *Brain*, *132*, 2487-2500.

Morita, S. & Miyata, S. (2012). Different vascular permeability between the sensory and secretory circumventricular organs of adult mouse brain. *Cell and Tissue research*, *349*, 589-603.

Murabe, Y., Nishida, K., & Sano, Y. (1981). Cells capable of uptake of horseradish peroxidase

in some circumventricular organs of the cat and rat. *Cell and Tissue Research*, *219*, 85-92.

Paloneva, J., Kestila, M., Wu, J., Salminen, A., Bohling, T., Ruotsalainen, V., . . . Peltonen, L. (2000). Loss-of-function mutations in TYROBP (DAP12) result in a presenile dementia with bone cysts. *Nature Genetics*, *25*, 357-361.

Paloneva, J., Manninen, T., Christman, G., Hovanes, K., Mandelin, J., Adolfsson, R., . . . Peltonen, L. (2002). Mutations in two genes encoding different subunits of a receptor signaling complex result in an identical disease phenotype. *American Journal of Human Genetics*, *71*, 656-662.

Paolicelli, R. C., Bolasco, G., Pagani, F., Maggi, L., Scianni, M., Panzanelli, P., . . . Gross, C. T. (2011). Synaptic pruning by microglia is necessary for normal brain development. *Science*, *333*, 1456-1458.

Parkhurst, C. N., Yang, G., Ninan, I., Savas, J. N., Yates, J. R., 3rd, Lafaille, J. J., . . . Gan, W. B. (2013). Microglia promote learning-dependent synapse formation through brain-derived neurotrophic factor. *Cell*, *155*, 1596-1609.

Pfrieger, F. W. & Slezak, M. (2012). Genetic approaches to study glial cells in the rodent brain. *Glia*, *60*, 681-701.

Prinz, M., Erny, D., & Hagemeyer, N. (2017). Ontogeny and homeostasis of CNS myeloid cells. *Nature Immunology*, *18*, 385-392.

Prinz, M. & Priller, J. (2014). Microglia and brain macrophages in the molecular age: from origin to neuropsychiatric disease. *Nature Reviews Neuroscience*, *15*, 300-312.

Prinz, M., Priller, J., Sisodia, S. S., & Ransohoff, R. M. (2011). Heterogeneity of CNS myeloid cells and their roles in neurodegeneration. *Nature Neuroscience*, *14*, 1227-1235.

Puttur, F., Arnold-Schrauf, C., Lahl, K., Solmaz, G., Lindenberg, M., Mayer, C. T., . . . Sparwasser, T. (2013). Absence of Siglec-H in MCMV infection elevates interferon alpha production but does not enhance viral clearance. *PLoS Pathogens*, *9*, e1003648.

Robinson, A. P., White, T. M., & Mason, D. W. (1986). Macrophage heterogeneity in the rat as delineated by two monoclonal antibodies MRC OX-41 and MRC OX-42, the latter recognizing complement receptor type 3. *Immunology*, *57*, 239-247.

Saederup, N., Cardona, A. E., Croft, K., Mizutani, M., Cotleur, A. C., Tsou, C. L., . . . Charo, I. F. (2010). Selective chemokine receptor usage by central nervous system myeloid cells in CCR2-red fluorescent protein knock-in mice. *PloS One*, *5*, e13693.

Sasmono, R. T., Oceandy, D., Pollard, J. W., Tong, W., Pavli, P., Wainwright, B. J., . . . Hume, D. A. (2003). A macrophage colony-stimulating factor receptor-green fluorescent protein transgene is expressed throughout the mononuclear phagocyte system of the mouse. *Blood*, *101*, 1155-1163.

Schafer, D. P., Lehrman, E. K., Kautzman, A. G., Koyama, R., Mardinly, A. R., Yamasaki, R., . . . Stevens, B. (2012). Microglia sculpt postnatal neural circuits in an activity and complement-dependent manner. *Neuron*, *74*, 691-705.

Schulz, C., Gomez Perdiguero, E., Chorro, L., Szabo-Rogers, H., Cagnard, N., Kierdorf, K., . . . Geissmann, F. (2012). A lineage of myeloid cells independent of Myb and hematopoietic stem cells. *Science*, *336*, 86-90.

Swinnen, N., Smolders, S., Avila, A., Notelaers, K., Paesen, R., Ameloot, M., . . . Rigo, J. M. (2013). Complex invasion pattern of the cerebral cortex bymicroglial cells during development of the mouse embryo. *Glia*, *61*, 150-163.

Takagi, H., Arimura, K., Uto, T., Fukaya, T., Nakamura, T., Choijookhuu, N., . . . Sato, K. (2016). Plasmacytoid dendritic cells orchestrate TLR7-mediated innate and adaptive immunity for the initiation of autoimmune inflammation. *Scientific Reports*, *6*, 24477.

Takagi, H., Fukaya, T., Eizumi, K., Sato, Y., Sato, K., Shibazaki, A., . . . Sato, K. (2011). Plasmacytoid dendritic cells are crucial for the initiation of inflammation and T cell immunity in vivo. *Immunity*, *35*, 958-971.

Tsuda, M. (2016). P2 receptors, microglial cytokines and chemokines, and neuropathic pain. *Journal of Neuroscience Research*.

Turnbull, I. R. & Colonna, M. (2007). Activating and inhibitory functions of DAP12. *Nature Reviews Immunology*, *7*, 155-161.

Varvel, N. H., Neher, J. J., Bosch, A., Wang, W., Ransohoff, R. M., Miller, R. J., & Dingledine, R. (2016). Infiltrating monocytes promote brain inflammation and exacerbate neuronal damage after status epilepticus. *Proceedings of the National Academy of Sciences of the United States of America*, *113*, E5665-5674.

Wang, Y., Cella, M., Mallinson, K., Ulrich, J. D., Young, K. L., Robinette, M. L., . . . Colonna, M. (2015). TREM2 lipid sensing sustains the microglial response in an Alzheimer's disease model. *Cell*, *160*, 1061-1071.

Wes, P. D., Holtman, I. R., Boddeke, E. W., Moller, T., & Eggen, B. J. (2016). Next generation transcriptomics and genomics elucidate biological complexity of microglia in health and disease. *Glia*, *64*, 197-213.

Wieghofer, P., Knobeloch, K. P., & Prinz, M. (2015). Genetic targeting of microglia. *Glia*, *63*, 1-22.

Willis, C. L., Garwood, C. J., & Ray, D. E. (2007). A size selective vascular barrier in the rat area postrema formed by perivascular macrophages and the extracellular matrix. *Neuroscience*, *150*, 498-509.

Yamasaki, R., Lu, H., Butovsky, O., Ohno, N., Rietsch, A. M., Cialic, R., . . . Ransohoff, R. M. (2014). Differential roles of microglia and monocytes in the inflamed central nervous

system. *Journal of Experimental Medicine*, *211*, 1533-1549.

Zhang, B., Gaiteri, C., Bodea, L. G., Wang, Z., McElwee, J., Podtelezhnikov, A. A., . . . Emilsson, V. (2013). Integrated systems approach identifies genetic nodes and networks in late-onset Alzheimer's disease. *Cell*, *153*, 707-720.

Zhang, J., Raper, A., Sugita, N., Hingorani, R., Salio, M., Palmowski, M. J., . . . Crocker, P. R. (2006). Characterization of Siglec-H as a novel endocytic receptor expressed on murine plasmacytoid dendritic cell precursors. *Blood*, *107*, 3600-3608.

Zimmermann, M. (1983). Ethical guidelines for investigations of experimental pain in conscious animals. *Pain*, *16*, 109-110.

Figure legends

FIGURE 1. Immunohistochemical specificity of Siglec-H antibody in mice.

(a–i) Antigen absorption test using recombinant Fc protein (a–c), Siglec-H-Fc (d–f) and Siglec-E-Fc (g–i). Immunoreactivity for Siglec-H (a,d,g, green) and Iba1 (b,e,h, red) in the cerebral cortex and the merged images (c,f,i) are shown. Images were acquired using the same laser power and sensitivity, and image processing were the same for Fc-, Siglec-H-Fc- and Siglec-E-Fc-reacted samples (a–c vs. d–f vs. g–i). (j–o) Immunoreactivity for Siglec-H in the cerebral cortex of WT (j–l) and *Siglech*$^{dtr/dtr}$ (m–o) mice. Immunoreactivity for Siglec-H (j,m, green) and Iba1 (k,n, red) in the cerebral cortex and the merged images (l,o) are shown. Images were acquired using the same laser power and sensitivity, and image processing were the same for WT and *Siglech*$^{dtr/dtr}$ samples (j–l vs. m–o). Scale bar: 50 μm.

FIGURE 2. Siglec-H is expressed by microglia but not by CNS-associated MΦ in adult mice, except for in the choroid plexus.

(a–d) Siglec-H expression in the surface region of the cerebral cortex. Immunoreactivity for Siglec-H (a, green) and CD206 (b, red), and the merged image of Siglec-H and CD206 (c) are shown. Meninges and vessels are visualized by laminin immunostaining (d, cyan). Microglia (arrows), pvMΦ (single arrowheads) and mMΦ (double arrowheads) are indicated. (e–h) Siglec-H expression in the surface region of the cerebral cortex. Immunoreactivity for Siglec-H (e, green) and CD206 (f, red), and the merged image of Siglec-H and CD206 (g) are shown. Iba1 immunostaining visualizes all myeloid cells (h, cyan). Microglia (arrows), pvMΦ (single arrowheads) and mMΦ (double arrowheads) are indicated. (i–l) Siglec-H expression in the area postrema of the medulla. Immunoreactivity for Siglec-H (i, green), CD206 (j, red) and Iba1 (l, cyan), and the merged image of Siglec-H and CD206 (k) are shown. Insets show higher magnification images of microglia (arrows) and cvoMΦ (arrowheads). An asterisk indicates a minor population that simultaneously expresses Siglec-H and CD206. (m–p) Siglec-H expression in the choroid plexus. Immunoreactivity for Siglec-H (m, green), CD206 (n, red) and Iba1 (p, cyan), and the merged image of Siglec-H and CD206 (o) are shown. Siglec-H$^+$/CD206$^-$ (arrows), Siglec-H$^-$/CD206$^+$ (arrowheads) and Siglec-H$^+$/CD206$^+$ (asterisks) cells are indicated. Scale bar: 50 μm, 15 μm (insets).

FIGURE 3. Siglec-H is expressed by microglia in the developing CNS of mice.

A, Developmental expression profile of mRNAs encoding Siglec-H and Iba1. mRNA levels in the cerebral cortex were analyzed by qPCR at each time point (n = 3 for each time point). Results are normalized to *Gapdh*, and shown as ratios to 8W mice. Values show the mean ± S.E.M. (b–g) Siglec-H expression in the developing cerebral cortex at E17 (b–d) and P7 (e–g).

Immunoreactivity for Siglec-H (b,e, green) and Iba1 (c,f, red), and the merged images (d,g) are shown. Scale bar: 50 µm. (h) Siglec-H^{+} rate (%) of Iba1^{+} cells in the cerebral cortex beneath the meninges at E17, P0 and P7 (n = 4; nine images per animal). Values show the mean ± S.E.M.

FIGURE 4. Siglec-H expression is absent from most infiltrating monocytes in the injured or inflamed CNS of mice.

(a–h) Siglec-H expression in the optic nerve of *Ccr2*$^{RFP/+}$ mice 7 days after crush injury. Siglec-H immunoreactivity (a,e, green) and RFP signal (b,f, red), the merged images of Siglec-H and RFP (c,g), and Iba1 immunoreactivity (d,h, cyan) of control (a–d) and injured (e–h) nerves are shown. Insets show higher magnification images of the injury site. Images were acquired using the same laser power and sensitivity, and image processing were the same for control and injured nerves (a–d vs. e–h). (i–p) Siglec-H expression in the ventral white matter of the spinal cord of *Ccr2*$^{RFP/+}$ mice with EAE. Siglec-H immunoreactivity (i,m, green), RFP signal (j,n, red), the merged images of Siglec-H and RFP (k,o), and Iba1 immunoreactivity (l,p, cyan) of control (naive: i–l) and EAE (m–p) mice are shown. Insets show higher magnification images. An asterisk indicates a minor population that simultaneously expresses Siglec-H and RFP. Images were acquired using the same laser power and sensitivity, and image processing were the same for naive and EAE mice (i–l vs. m–p). Scale bar: 50 µm, 10 µm (insets).

FIGURE 5. Siglec-H expression is absent from infiltrating monocytes in the injured PNS of mice.

(a–i) Siglec-H expression in the spinal cord (a–f) and in the distal part of the injured nerve (g–i) 7 days after sciatic nerve transection. Areas indicated by white squares in low magnification images (a–c) are shown as higher magnification images (d–f). Immunoreactivity for Siglec-H (a,d,g, green) and Iba1 (b,e,h, red), and the merged images (c,f,i) are shown. Images were acquired using the same laser power and sensitivity, and image processing were the same for dorsal horn and sciatic nerve samples (d–f vs. g–i). (j) Expression changes of mRNAs encoding Siglec-H and Iba1 in the dorsal horn 7 days after sciatic nerve transection (n = 3). The contralateral (contra) and ipsilateral (ipsi) dorsal horns were subjected to qPCR. Results are normalized to *Gapdh*, and shown as ratios to the contralateral side. Values show the mean ± S.E.M. (k) Expression changes of mRNAs encoding Siglec-H and Iba1 in the sciatic nerve 7 days after transection (n = 3). The contralateral (contra) and ipsilateral (ipsi) sciatic nerves were subjected to qPCR. Results are normalized to *Gapdh*, and shown as ratios to the contralateral side. Values show the mean ± S.E.M. *$p < 0.005$ and **$p < 5.0 \times 10^{-4}$ for upregulation, $^{\#}p < 0.05$ for downregulation; unpaired Student's t-test.

FIGURE 6. DT administration specifically ablates microglia in *Siglech*$^{dtr/dtr}$ mice.

(a–i) DT induces microglial ablation in the cerebral cortex (a–e) and the area postrema (area surrounded by dotted line, f–i) of non-injured adult *Siglech*$^{dtr/dtr}$ mice 2 days after administration. Merged images of Iba1 (green) and CD206 (red) immunostaining of PBS- (a,f) and DT- (b,g) treated mice are shown. The numbers of Iba1^{+}/CD206^{-} microglia (c,h), CD206^{+} pvMΦ (d), CD206^{+} mMΦ (e) and CD206^{+} cvoMΦ (i) are quantified (n = 3; four images per animal). (j–l) DT induces microglial ablation in the dorsal horn of sciatic nerve-injured adult *Siglech*$^{dtr/dtr}$ mice 2 days after administration. Merged images of Iba1 (green) and PKCγ (red) immunostaining of PBS- (j) and DT- (k) treated mice are shown. Lamina I/IIo is surrounded by a dotted line. Iba1^{+} microglial numbers in lamina I/IIo of contralateral (contra) and ipsilateral (ipsi) dorsal horn are quantified (l) (n = 3; four images per animal). (m–o) DT does not affect the number of monocytes/MΦ accumulated in injured sciatic nerve of adult *Siglech*$^{dtr/dtr}$ mice 2 days after administration. Monocytes/MΦ are stained with anti-Iba1 antibody (green) in the ipsilateral sciatic nerve of PBS- (m) and DT- (n) treated *Siglech*$^{dtr/dtr}$ mice. Iba1^{+} areas of contralateral (contra) and ipsilateral (ipsi) sciatic nerve were quantified from images taken with the same laser power and microscope sensitivity (o) (n = 3; four images per animal). Values are normalized to the whole area, and are shown as ratios to the contralateral nerve of the PBS-administrated group. (p–r) DT induces microglial ablation in the cerebral cortex of P7 *Siglech*$^{dtr/dtr}$ mice 2 days after administration. Merged images of Iba1 (green) and laminin (red) immunostaining of PBS- (p) and DT- (q) treated mice are shown. Putative pvMΦ (single arrowheads) and mMΦ (double arrowheads) are indicated. The number of Iba1^{+} cells in the cerebral cortex beneath the meninges is quantified (r) (n = 3; four images per animal). Scale bar: 200 μm (a,b,f,g,j,k,m,n), 50 μm (p,q). *$p < 0.001$, **$p < 1.0 \times 10^{-4}$; unpaired Student's t-test.

FIGURE 7. Siglec-H suppresses pro-inflammatory responses of microglia in a mouse neuropathic pain model.

(a) Expression profile of mRNA encoding Siglec-H in the dorsal horn. Ipsilateral dorsal horn was obtained from WT and *Siglech*$^{dtr/dtr}$ mice at each time point after L4 nerve transection, and mRNA expression was analyzed by qPCR (n = 3 for each time point). Results are normalized to *Gapdh*, and are shown as ratios to the non-operated (naive) value of WT mice. Values show the mean ± S.E.M. *$p < 0.05$, **$p < 0.005$; unpaired Student's t-test. (b–j) Expression of Siglec-H protein in the ipsilateral dorsal horn 3 days after L4 nerve injury. Immunoreactivity for Siglec-H (b,e,h, green) and Iba1 (c,f,i, red), and the merged images (d,g,j) of WT (b–g) and *Siglech*$^{dtr/dtr}$ (h–j) mice are shown. Higher magnification images of WT mice (e–g, high mag.) demonstrate Siglec-H expression in microglia. Note that faint signals for Siglec-H are predominantly

observed in the endoplasmic reticulum/Golgi apparatus of microglia in *Siglech*$^{dtr/dtr}$ mice (arrows in h–j, high mag.). Images were acquired using the same laser power and sensitivity, and image processing were the same for WT and *Siglech*$^{dtr/dtr}$ mice (e–g vs. h–j). Scale bar: 200 μm (b–d), 10 μm (e–j). (k) Expression of mRNA encoding pro-inflammatory cytokines (TNF-α and IL-1β) but not anti-inflammatory cytokines (IL-10 and TGF-β1) was upregulated in the ipsilateral dorsal horn of *Siglech*$^{dtr/dtr}$ mice. Ipsilateral L4 dorsal horn was obtained from WT and *Siglech*$^{dtr/dtr}$ mice at each time point after L4 nerve transection ($n = 3$ for each time point), and mRNA expression was analyzed by qPCR. Results are normalized to *Gapdh*, and are shown as ratios to the non-operated (naive) value of WT mice. Values show the mean ± S.E.M. $*p < 0.05$, $**p < 5.0 \times 10^{-4}$; unpaired Student's *t*-test. (l–n) Microglial numbers in lamina I/IIo were unchanged between WT and *Siglech*$^{dtr/dtr}$ mice 7 days after injury. Merged images of Iba1 (green) and PKCγ (red) immunostaining of WT (l) and *Siglech*$^{dtr/dtr}$ (m) mice are shown. The lamina I/IIo is surrounded by dotted lines. Scale bar: 200 μm. Microglial numbers in lamina I/IIo of contralateral (contra) and ipsilateral (ipsi) L4 dorsal horn were counted at 7d (n) ($n = 4$; four images per animal). (o,p) Nerve injury-induced mechanical allodynia is exacerbated in *Siglech*$^{dtr/dtr}$ mice. The PWT of the contralateral (o) and ipsilateral (p) side was measured in WT and *Siglech*$^{dtr/dtr}$ mice ($n = 4$). $*p < 0.05$; two-way ANOVA with *post hoc* Bonferroni test.

Figure 1. Konishi et al.

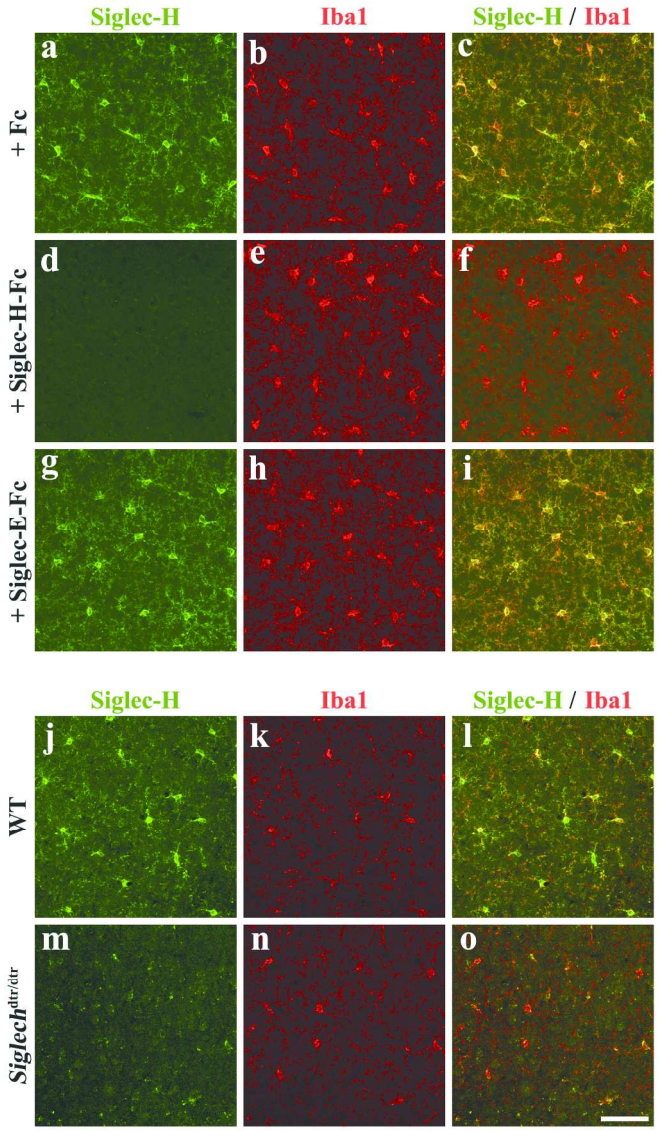

Fig1_Konishi

129x238mm (300 x 300 DPI)

Figure 2. Konishi et al.

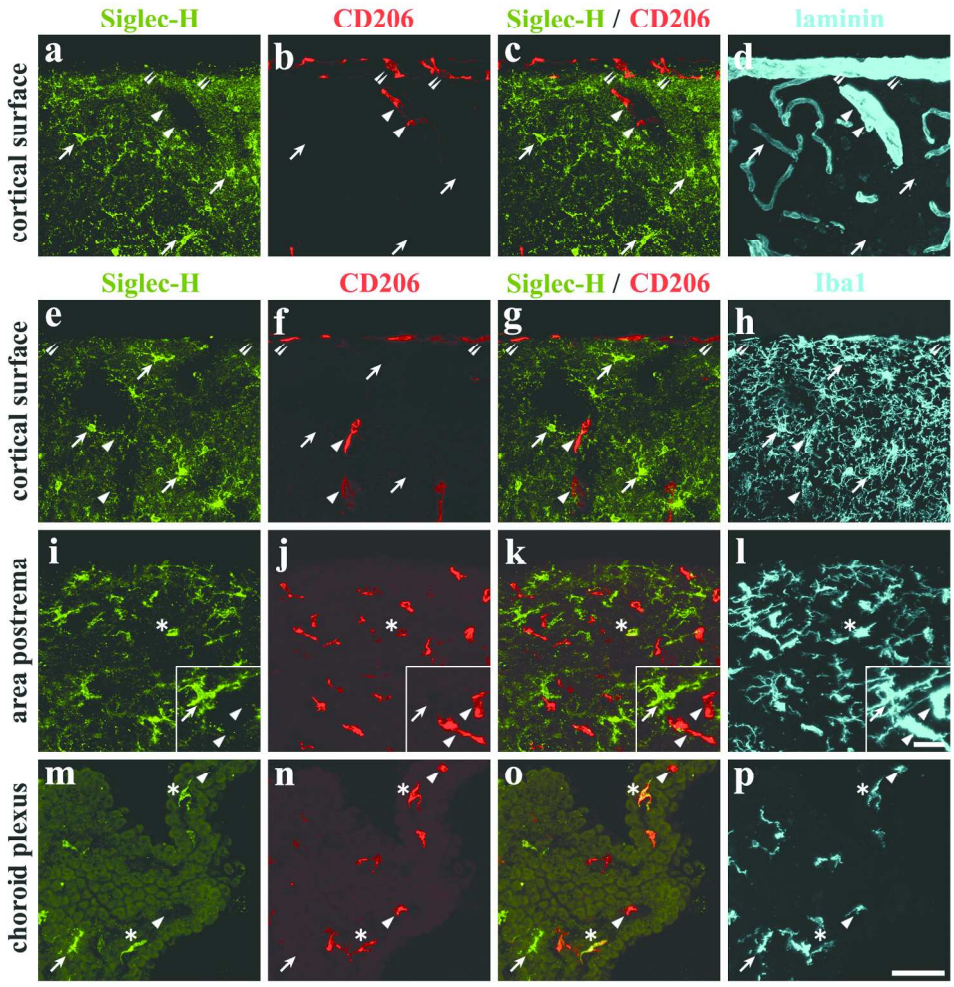

Figure 2

180x191mm (300 x 300 DPI)

Figure 3. Konishi et al.

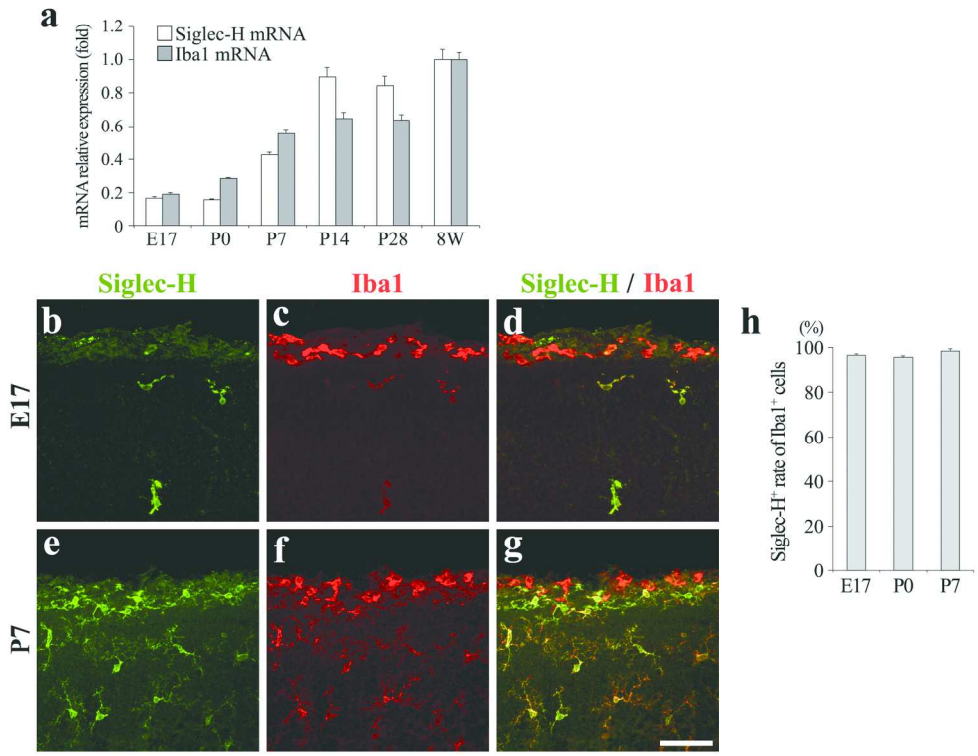

Figure 3

180x150mm (300 x 300 DPI)

Figure 4. Konishi et al.

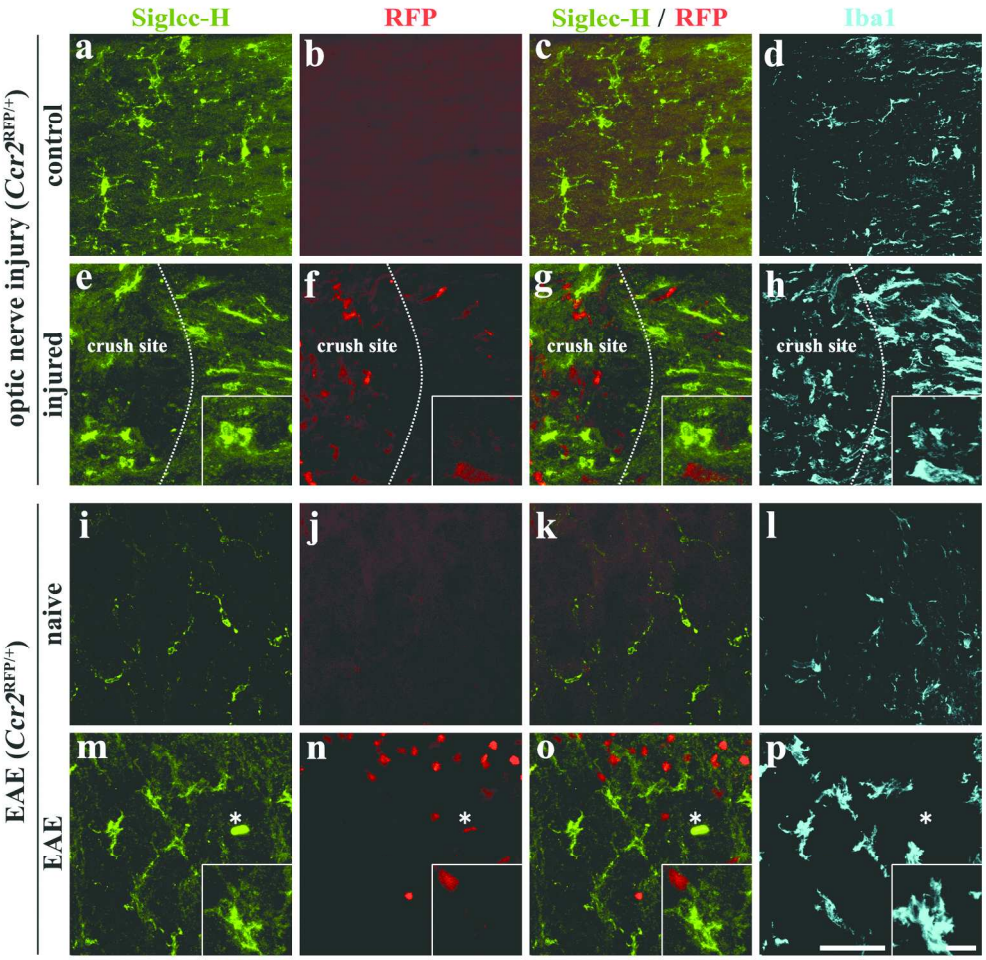

Fig4_Konishi

180x187mm (300 x 300 DPI)

Figure 5. Konishi et al.

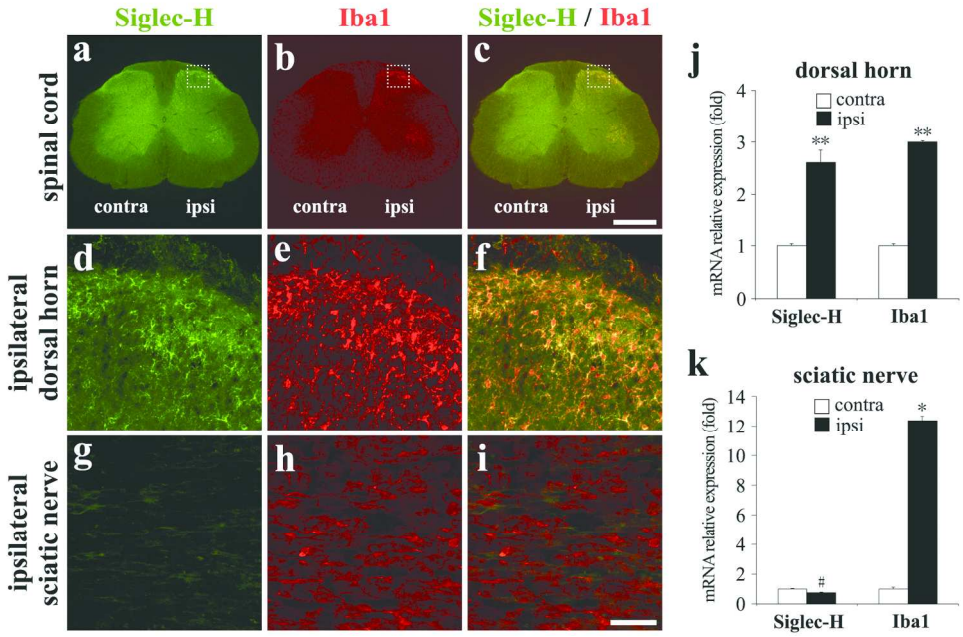

Figure 5

180x128mm (300 x 300 DPI)

Figure 6. Konishi et al.

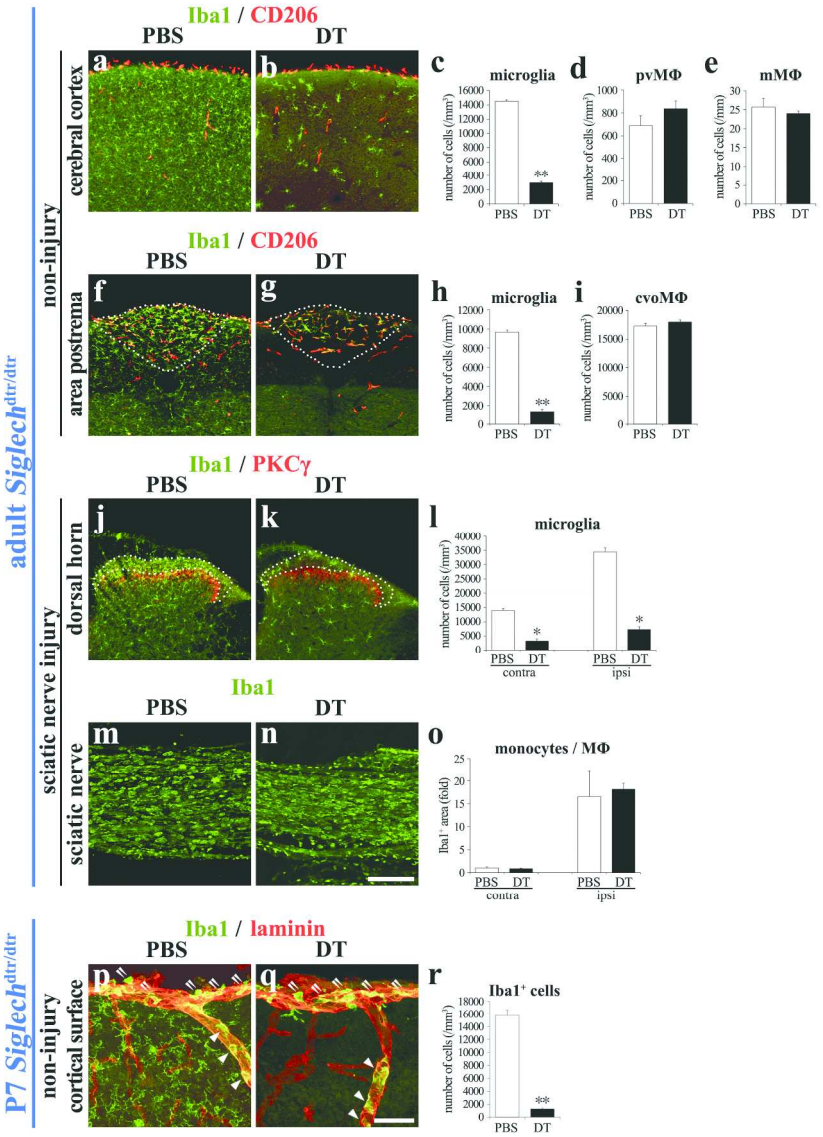

Figure 6

180x258mm (300 x 300 DPI)

Figure 7. Konishi et al.

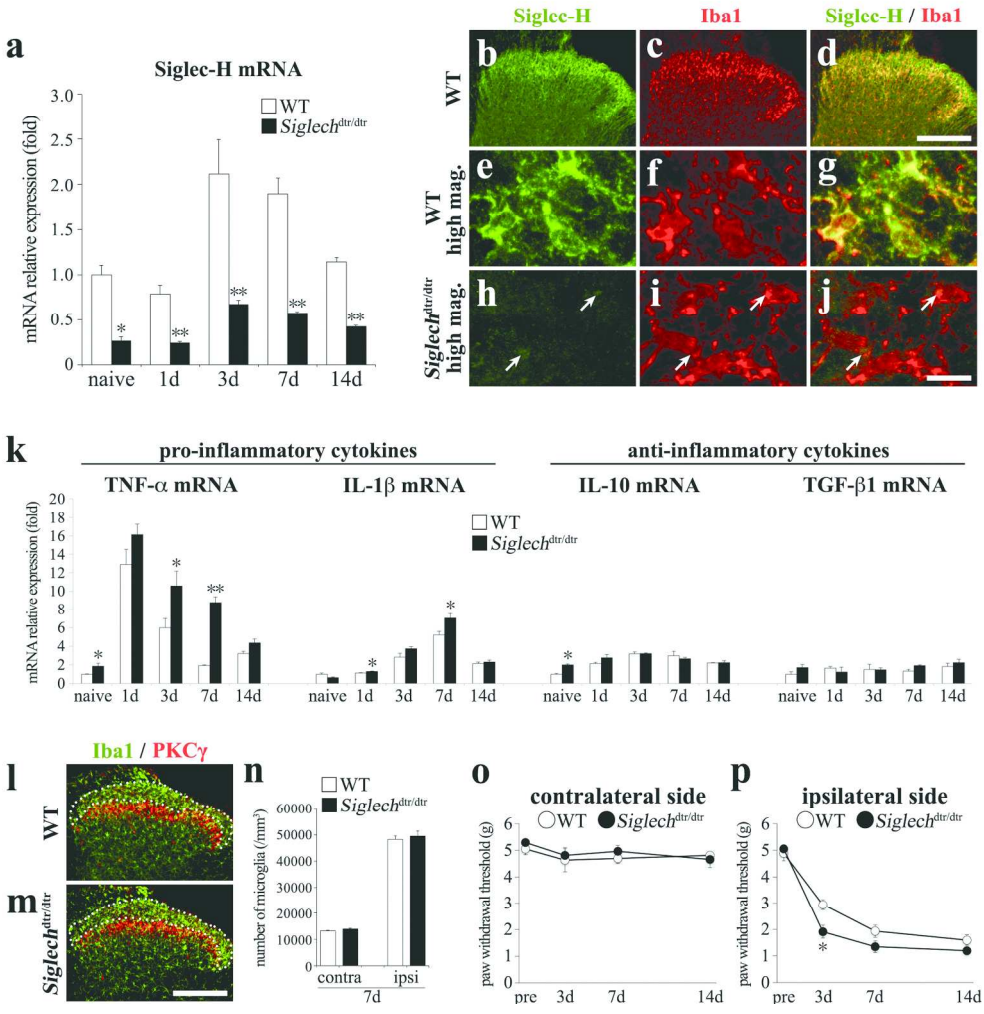

Figure 7

180x194mm (300 x 300 DPI)

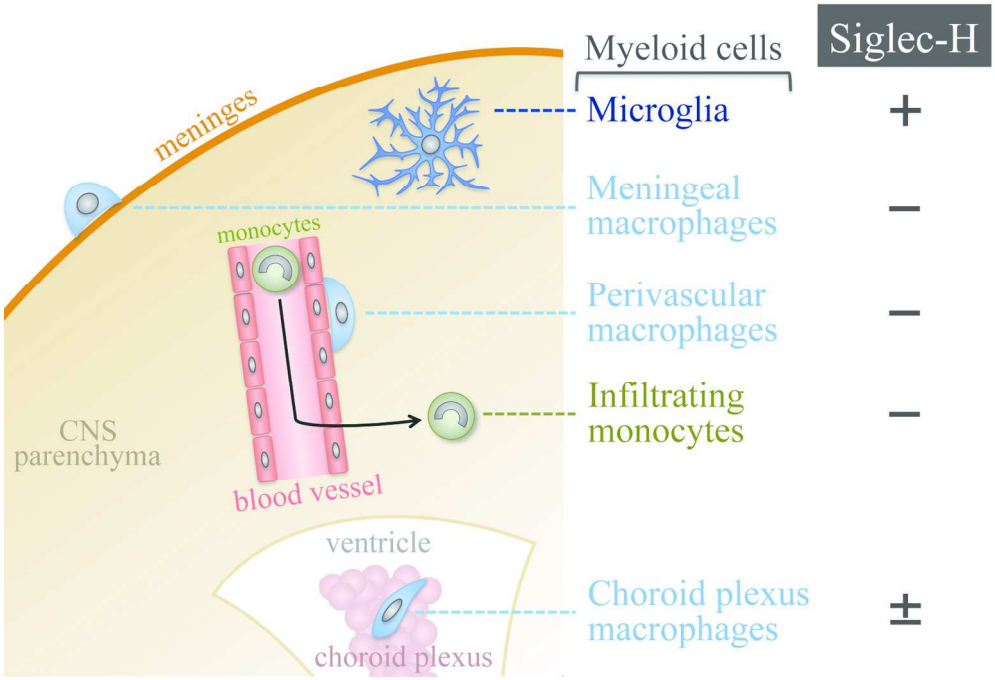

TOCI_Konishi

153x105mm (300 x 300 DPI)

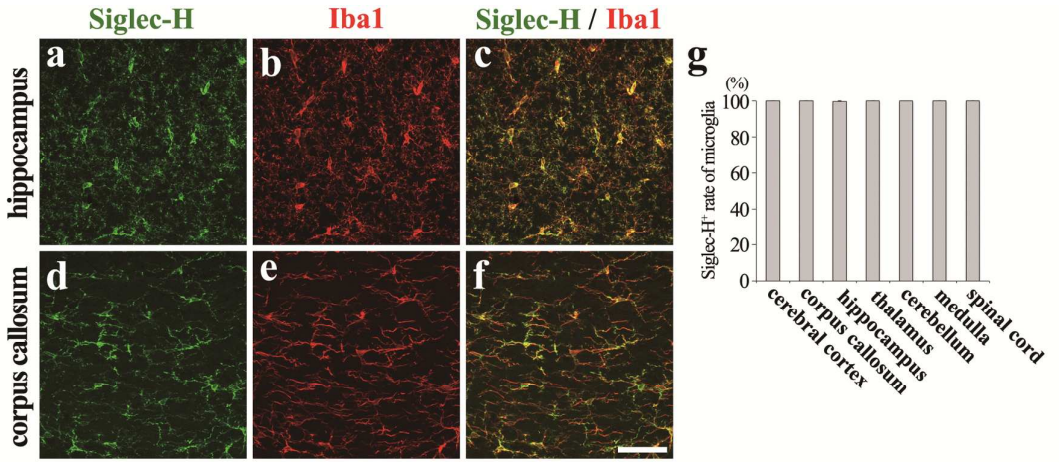

FIGURE S1. Siglec-H is expressed by microglia throughout the CNS of adult mice.

(a–c) Siglec-H expression in the CA1 region of the hippocampus. Immunoreactivity for Siglec-H (a, green) and Iba1 (b, red), and the merged image (c) are shown. (d–f) Siglec-H expression in the corpus callosum. Immunoreactivity for Siglec-H (d, green) and Iba1 (e, red), and the merged image (f) are shown. Scale bar: 50 μm. (g) Siglec-H^+ rate (%) of $Iba1^+$ parenchymal microglia in indicated regions of the CNS (n = 4; nine images per animal). Values show the mean ± S.E.M.